Optical Imaging and Spectroscopy of Airborne Nanowires

Eleni Gompou

Master's Thesis
2017

LUND
UNIVERSITY

Division of Solid State Physics
Department of Physics
Lund University

Master's thesis which, by due permission of the Faculty of Science at Lund University, Sweden, was publicly defended on Wednesday, January 12, 2017 for the degree of Master's in Physics, Nanoscience.

Examiner: Claudio Verdozzi
Supervisor: Martin Magnusson
Lund University

Acknowledgements

I am extremely thankful to my supervisor Martin Magnusson for his constant support and encouragement. He always succeeds in creating a joyful mood even when the things in the lab are not going the right way.

Many thanks to the Aerotaxy team, Wondwosen Metaferia and Sudha Sivakumar who were always willing to help with my experiments despite that I was irritating them a lot. I would also like to thank Per Samuelsson and Niklas Sköld for helping me to assemble my set up and Enrique Barrigon and Nicklas Anttu for giving some really good advices. I am really thankful to Bengt Meuller who contributed in the assembling of my system and kept it running. Many sincere thanks to Dan Hessman who spent so much time in the lab with me and shown light in my dark PL spectrum!

I would like to thank all the office mates for creating a joyful and distressful environment. Vishal and Ali thank you for the generous support when it was most needed it. Shishir the only thing that I can say here is that I really thank you for deciding to come in Lund. I had to come in Sweden to find such a unique person as you!

Mum dad and Andrea thank you for your love and support. You are always next to me even though you are so far away!

Abstract

Semiconductor nanowires are the potential base for building many future devices like solar cells and light emitting diodes. To reach the level of commercialization of such devices, mass production of NWs at low cost with reproducible high quality properties in terms of crystallinity, material and dimensions is a prerequisite. At Lund University a new technique, called Aerotaxy, which satisfies these characteristics, has been developed for continuous production of nanowires in the aerosol phase.

Further optimization of Aerotaxy process created the need for in situ, on line and on real time characterization of the aerosol NWs for a quick feedback during growth. For this purpose, I created a new set up for checking the feasibility of photoluminescence spectroscopy, absorption spectroscopy and imaging of the nanowire flow using the polarized and unpolarized scattered light. PL and absorption spectroscopy would be conducted for quality check of nanowires. Furthermore, absorption spectrum from aligned nanowires could possibly give information about their diameter and scattering from aligned nanowires would be tested for correlating the electric field strength used for aligning them to their length. Moreover, imaging of unpolarized scattered laser light would give us information on fluctuations in nanowire flow.

Due to insufficient set up components like fiber spectrometer, with poor signal collection efficiency and low quantum efficiency of the chip, in situ PL spectroscopy could not be performed. Scattering of laser light is successfully used for visualizing the nanowire flow which gives an immediate feedback on when the growth is taking place. Scattering experiments of polarized scattered light showed an effect on the direction of the nanowires but because of insufficient number of experiments no conclusions can be drawn. No conclusions also can be drawn for absorption experiments.

Abbreviations

Au	Gold
CBE	Chemical Beam Epitaxy
GaAs	Gallium Arsenide
InAs	Indium Arsenide
InP	Indium Phosphide
LED	Light Emitting diode
MBE	Molecular Beam Epitaxy
MOVPE	Metal Organic Vapor Phase Epitaxy
NW	Nanowire
PL	Photoluminescence
Si	Silicon
VB	Valence Band
CB	Conduction Band
Zn	Zinc
NP	Nanoparticles
nm	nanometers
μm	micrometers

Contents

1 Introduction

It would be hard to imagine our world, which is more and more dominated by devices, without semiconductors. Due to their properties, semiconductors are the base for electronic devices such as transistors, LEDs, solar cells, lasers and detectors. Since the first transistor was invented in 1948 the advance in solid state devices has been tremendous not only because of the progress of device designing but also because of the evolution of material synthesis [1]. Growing pure single crystal Si in 1950 made integrated circuits feasible and Si became a dominant material in electronics [1]. Henceforth, the development of diverse growing techniques has led to an increasing control on the material synthesis and of material properties as well. Nowadays, the semiconductor industry is leading progressively in replacing Si with III-Vs such as GaAs, InP, and InAs because of their better electronic and optical properties such as higher electronic mobilities as well as higher optical absorption and optical emission efficiencies [2,3].

The need for lower cost, higher powers and better performance, along with the fact that availability of certain materials is restricted, have led towards to the miniaturization of devices. Towards this direction, nanotechnology has opened the way for designing new materials and structures on atomic scales. In this size regime materials have different properties from those of the bulk and thin films. Due to quantisation effects which become really prominent, their properties are highly dependent on their size and shape as well. Moreover, high surface-to-volume ratio is another important factor that differentiates nanostructures from the bulk.

Semiconductor nanowires are one dimensional rod like nanostructures with high aspect ratio – their diameter is in the range of a few nanometers to a few hundreds of nanometers, and their length is about 1–10 microns [4]. They have drawn the interest of research for more than 20 years due to the unique photonic, electronic and mechanical properties which make them ideal candidates for the majority of electronic devices [4]. Crystal structures unstable in the bulk manifest stability in nanowires, which can pave the way for devices with different properties made of the same material. As an example, we can mention III–Vs which form a mix of zincblende and wurtzite crystal structure in nanowires while the majority of them only appear in zinc blend structure in the bulk [5]. Moreover different types of heterostructures can be achieved because of their small diameter which permits radial strain relaxation, forbidden in conventional planar structures due to lattice mismatch. As a result, a big span of different materials can be combined to form heterojunctions free from defects [5,6]. This characteristic is really important for quantum dots because it enables the growth of nanowires from a material with small band gap containing parts of larger band gap thereby creating electron confinement [7]. It also opens the way for tandem solar cells which have multiple heterojunctions and makes possible the successful integration of III–Vs on Si substrates, which currently dominate the industry [7]. Another advantage of nanowires with respect to

solar cell applications is that they interact in such a way with light when they are periodically and vertically arranged that they can have similar absorption efficiency with conventional thin films [8]. Consequently, NWs are promising candidates for photovoltaics (PV) as the amount of material used is smaller than in planar structures.

1.1 Aerotaxy

At Lund University, a novel technique of continuous production of NWs in the aerosol phase has been developed. It is a tool which makes feasible the growth of large amounts of NWs with reproducible properties. By controlling the growth temperature, the size of gold nanoparticles and the growth time, the length, the diameter and the shape of NWs can be controlled respectively, although temperature affects their shape as well [9]. NW diameters range between 20 and 80 nm while their length can reach up to 6 μm with a length variation down to ±10% [9].

Compared to other epitaxial methods, Aerotaxy has many advantages. No substrate is needed for the growth so production cost is much lower [9]. The axial growth rate of aerosol NWs is 1 μm/second which makes Aerotaxy almost three orders of magnitude faster than the previous mentioned techniques [9]. Furthermore, the number of produced NWs in substrate based techniques is limited by the size of the substrate – which is not the case for Aerotaxy. The combination of this factor with the high growth rate of aerosol NWs increases the throughput of Aerotaxy. To the previous advantages, we can also add the possibility of high Zn doping concentration which reaches up to 10^{20} cm^{-3} [10]. These high levels of doping are not feasible in MOVPE due to diffusion of dopants to the substrate. As a result, Aerotaxy seems to be a promising tool for mass production of NWs which could enable their use for commercial applications in the future.

1.2 Purpose of the project

The aim of this project is the creation of a set-up for conducting on line, *in situ* and in real time optical characterization of aerosol NWs produced from Aerotaxy. For this purpose, the experimental set-up is placed between the growth furnace and the deposition chamber, so that experiments are conducted after the completion of the nanowire growth and before the deposition. The optical tools used for characterization are imaging from elastic scattering of monochromatic laser light; photoluminescence (PL) spectroscopy and absorption spectroscopy of visible and infrared light. By detecting the scattered laser light with a CCD camera we can derive information about the concentration of the NWs in the aerosol flow since the scattered light is proportional to their number. Moreover, information about their length can be derived from scattering experiments if the NWs are aligned by applying electric field. This can be done by detecting the intensity of light with polarization parallel to the axis

of completely aligned NWs. PL spectroscopy will make the real time monitoring of the possible doping and provide a feedback of the quality of material from the spectral position of PL peak and its intensity, respectively. Absorption spectroscopy will also provide us with information concerning the quality of nanowires since a ´´step like`` decrease in the transmitted signal is expected at wavelength corresponding to the band gap energy. Furthermore, we are expecting absorption resonances depending on the nanowire diameter when they are aligned and considering that they are spaced in distances bigger than the wavelength so that there is no interaction among them. This phenomenon has been experimentally observed in photocurrent measurements from single Ge nanowires [11] and confirmed from simulations for GaAs [12] and Si [13] nanowires.

The development of such a tool is important for the optimization of a continuous process as it can give real time feedback without disturbing the aerosol flow. In this way changes in the growth parameters can be adjusted during growth so that desirable characteristics of NWs are achieved. For the time being, these adjustments have to be done *ex situ* which makes the optimization process time consuming.

In addition, doing *in situ* PL spectroscopy has the advantage of investigating the unoxidized NWs because there is no oxygen in the tube. This is a very important factor since GaAs is very easily oxidized which deteriorates the PL signal. On the other hand, the fact that they are not passivated, which also deteriorates the PL signal should not be neglected.

2 Background

2.1 Semiconductors

Semiconductors are a group of solid state materials with crystalline structure which has electrical conductivities in the range of values between metal conductivities (10^4–10^6 S/cm) and insulator conductivities (10^{-18}-10^{-8} S/cm) and that also increase under illumination, doping and increase of temperature [14]. This characteristic is determined from the energy band structures of these materials. It is the result of the combination of the energy states of atoms when they are brought together to form the crystal lattice and the way that the conduction and valence bands are occupied by electrons.

In insulators, the conduction band (the lowest unoccupied band) is completely empty while the valence band (the highest occupied band) is completely full with electrons. They are separated by a very large energy bandgap where there are no energy states at all. When an electric field is applied, there are no vacant energy states in the valence band for the electrons to move. Since the band gap is very big – on the order of 9 eV – the kinetic energy gained from the electric field or from thermal energy is not enough for a significant number to be raised to the conduction band, which results in very low conductivities [14]. In metals, there are two possible structures: either the conduction band overlaps the valence band or the conduction band is only partially filled. In both these cases, a small increase in the kinetic energy of the electrons is enough for them to move to states with higher energy, which results in very high conductivities.

Coming now to semiconductors at very low temperatures – on the order of 0 K – they also have a filled valence band and an empty conduction band separated by an energy band gap just like in insulators. What differentiates them is the smaller band gap which is on the order of 1 eV [14]. Electrons with the highest energies can be easily excited to the conduction band, for example thermally (at room temperature) or optically. Excitation of carriers leads to the intermediate and highly variable values of semiconductor conductivities between metals and insulators. Also their conductivity and their optical properties can be controlled from introduction of impurities to them by doping.

2.1.1 Band structure

There are two types of semiconductor: those with direct band gap like most III–Vs, in which the conduction band minimum lies at the same wavenumber value k as the valence band maximum. The other type is indirect band gap semiconductors, such as Si, in which CB

minimum and VB maximum are at different k values. This is a significant characteristic when it comes to optoelectronic devices because it affects the absorption and emission of photons.

Radiative emission happens when one electron recombines with one hole to release one photon which has energy equal to the bandgap energy. A photon carries a very small momentum, so in the band diagram such a transition is vertical. In the direct band gap materials both energy and momentum are conserved for transitions from the bottom of the conduction band to the top of the valence band, where more electrons and holes reside respectively. To the contrary the emission of only a photon which does not carry momentum is not enough for the conservation of momentum, and a phonon needs to participate. So, in indirect materials, for energy and momentum conservation an electron, a hole, a photon and a phonon need to participate simultaneously which makes the process less probable than in direct bandgap materials [2]. This is the reason why III-Vs are preferred for optoelectronic devices like lasers or LEDs.

In the same way, in direct band gap semiconductors absorption happens for energies equal or larger than the band gap energy. To the contrary, in the case of indirect bandgap materials energy needs to be larger than E_g since vertical transitions correspond to higher energies as it can be seen in the Figure 2.1. Consequently devices made of indirect bandgap materials are transparent for bigger energy range and excited electrons ending up in the CB are thermalized- an unwanted side effect for solar applications [6].

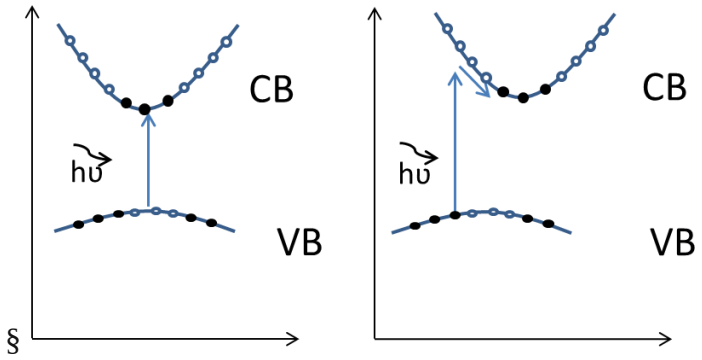

Figure 2.1*: E-k band diagrams for (a) direct band gap materials and (b) indiret bandgap materials with arrows showing the possible absorption transitions. Black dots represet the electrons and white dots the holes.*

2.1.2 Charge carriers in semiconductors

Semiconductors with perfect lattice crystals, meaning no impurities or free from defects, are called intrinsic and at 0 K they have no free charge carriers as it is explained above. But when the temperature is higher than 0 K, charge carriers are created from thermal excitation. These carriers are electrons migrating in the conduction band and holes which are empty states in the valence band. Mathematically this phenomena can be explained by the Fermi – Dirac

distribution which describes the occupation probability of a state with energy E by an electron or a hole carrier:

$$F_e(E) = \frac{1}{1+e^{\frac{E-E_F}{kT}}} \quad (1)$$

$$F_h(E) = \frac{1}{1+e^{-\frac{E-E_F}{kT}}} \quad (2)$$

$F_e(E)$: is the Fermi – Dirac distribution for holes and $F_h(E)$: is the Fermi – Dirac distribution for holes [1]. As it can be seen the probability that an electron is in a state with higher energy is inversely proportional to the temperature and this is the reason why at higher temperature there are more electrons at higher energies. Similarly, at higher temperature there is higher probability for holes to occupy stetes deeper in the valence band. Both types of carriers contribute to the current when an electric field is applied. In intrinsic semiconductors, the electrons and holes are equal in number but not that many.

The way to increase the number of charge carriers, and consequently the conductivity of materials, is by introducing impurities to them. This technique is called doping, and the lattices are no longer perfect. As a result, energy states are created in the band gap. Depending on the dopant elements, additional states are either empty energy states close to the valence band or full states close to the conduction band. Room temperatures are more than enough in the first case for electrons to move from the valence band and fill all of the dopant states or in the second case for electrons to empty the dopant states by migrating to the conduction band [14]. This can be seen schematically in the figure 2.2. So, if doping concentrations are much higher than the intrinsic charge concentrations, materials have much higher conductivities and they are called n-doped or p-doped depending on the impurities.

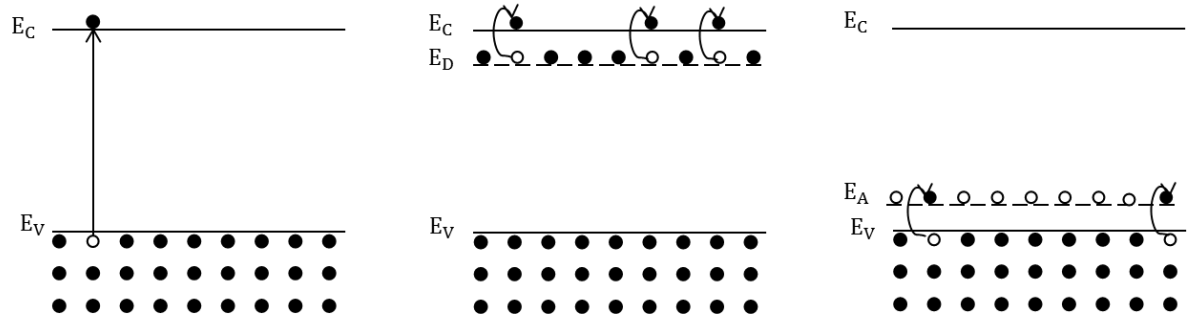

(a) intrinsic *(b) n - doped* *(c) p - doped*

***Figure 2.2**: Schematics of energy states at room temperatures of (a) intrinsic material (b) n-doped materials (c), p-doped materials.E_C: conduction band edge E_V: valence band edge, E_D: Donor states, E_A: acceptor states. The black dots are electrons and white dots are holes.*

2.2 Alignment of aerosol NWs in electric field

Semiconductor nanowires in external electric field can be treated as infinite semiconducting cylinders [15]. This means that the parallel component to the nanowire axis of the electric field, E_p, inside the nanowire is equal to the parallel component to the nanowire axis of the external electric field $E_{o,p}$, as it is expected from boundary conditions of Maxwell equation [16]:

$$E_p = E_{o,p} \tag{3}$$

On the contrary the normal component to the wire axis, E_n, in the nanowire is smaller than the normal component to the wire axis of the external electric field, $E_{o,n}$ [15] :

$$E_n = \frac{2\varepsilon_o}{\varepsilon+\varepsilon_o} E_{o,n} \tag{4}$$

In our experiments the GaAs nanowires are inside Nitrogen flow so the dielectric constant of the medium is $\varepsilon_o \approx 1$ and the dielectric constant of the nanowires is $\varepsilon = 12.4$ [14]. After calculations, the electric field component perpendicular to the wire axis in the nanowire is much smaller than the relevant component of the external electric field: $E_n = 0.14E_{o,n}$. As a result, when electric field is applied, an electric dipole moment is induced parallel to the nanowire axis because of two reasons: free carriers - electrons and holes - drift in opposite directions along electric field lines and lattice charges diverge from their fixed positions. If the electric field is uniform and the nanowire axis is not oriented parallel to the external electric field, a torque will exerted on the nanowire which will rotate it and tend to align it parallel to E_o. as shown in figure 2.3.

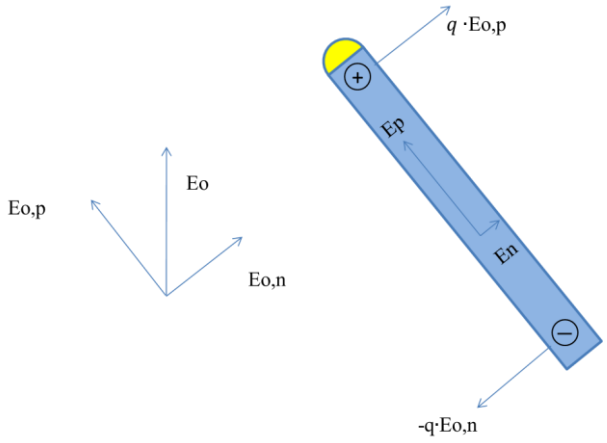

***Fifure2.3**: Shows the electric field E_o outside the nanowire and the electric field components normal and parallel to the nanowire axis outside and inside the nanowire: $E_{o,p}$, $E_{o,n}$ E_p, E_n. We see also the force exerted on the nanowire which results in its rotation*

The potential energy of a nanowire in electric field with its axis in angle θ with respect to electric field lines is given from equation (4) using the approximation that it has ellipsoidal shape [18].

$$\Phi = -\frac{1}{2}(2\pi\varepsilon_o)V{E_o}^2[\frac{\cos^2\theta}{1/(\varepsilon-1)+k_1} + \frac{\sin^2\theta}{1/(\varepsilon-1)+k_2}] \quad (5)$$

In equation (5) ε_o is the vacuum permittivity, ε is the dielectric constant of the nanowires, *V* is the volume of the nanowire, E_o is the external electric field, k_1 and k_2 shape factors related to the aspect ratio of nanowire length to the nanowire diameter d, and θ is the angle of nanowires with respect to the electric field lines. Considering now a moving aerosol system with laminar flow, the alignment of nanowires becomes possible only when the energy due to interaction of the dipoles with the electric field is higher than the thermal energy related to the Brownian motion tending to randomize their orientation [18]. More specifically, Fuchs [19] proposed that the electric energy should be at least ten times higher than thermal energy for alignment to be achieved. In figure 2.4 we see the electric energy relative the Brownian rotation energy as a function of applied electric field.

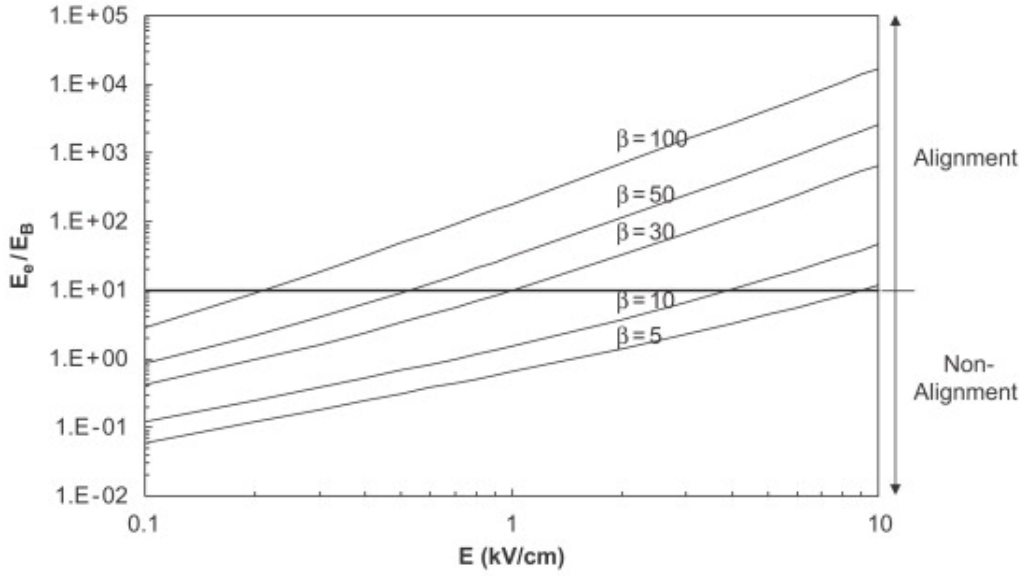

Figure2.4: The figure shows the relative electrical energy to Brownian rotation energy as a function of applied electric feild and aspect ratio β of the nanowires (here the NW diameter is assumed to be 15 nm and only the length changes)[14]

As we can see in figure 2.4, the alignment of the nanowires depends on the dimensions of the nanowires and more specifically on their aspect ratio [18]. Stronger electric fields are needed for NWs with smaller aspect ratios than for those with bigger aspect ratios as shown in the same figure [18].

2.3 Interaction of light with nanowires

2.3.1 Absorption and scattering of light from NWs

The interaction of light with subwavelength semiconducting particles creates resonant effects. More specifically NWs with diameters much smaller than the wavelength of the incident light act like cylindrical cavity antennas which can trap light in circulating orbits by total internal reflections from their periphery [11,20,21]. In other words, incident light is coupled to leaky mode resonances supported by the nanowire and this results in enhancement of specific wavelengths for both scattered and absorbed light. Modes are electromagnetic fields which keep the same transverse polarization and amplitude along the nanowire axis [2] and leaky modes are electromagnetic fields which propagate outside the nanostructures [12]. In the case of nanowires, the leaky modes are due to the much smaller radius compared to the light wavelength. Since the NWs are very long compared to the effective wavelength of light in the material-which is the wavelength in vacuum devided by the refractive index of the material-, resonances are not affected by their length [13].

Using classical waveguide theory the eigenvalues of leaky modes can be calculated from equation (6) which is derived from Maxwell's equations assuming infinitely long NWs [11]:

$$\left(\frac{1}{\gamma_w^2}-\frac{1}{\gamma_a^2}\right)^2\left(\frac{\beta m}{a}\right)^2 = k_a^2\left(n_w^2\frac{J_m'(\gamma_w a)}{\gamma_w J_m(\gamma_w a)} - n_a^2\frac{H_m'(\gamma_a a)}{\gamma_a H_m(\gamma_a a)}\right)\times\left(\frac{J_m'(\gamma_w a)}{\gamma_w J_m(\gamma_w a)} - \frac{H_m'(\gamma_a a)}{\gamma_a H(\gamma_a a)}\right) \quad (6)$$

In equation (6), J_m, H_m are the m:th order Bessel and Hankel functions respectively of the first kind and J_m', H_m' are their first derivatives, k_w and k_a are the wavevectors of light inside and outside the NW respectively, γ_w and γ_a are the vertical components of k_w and k_a respectively, and β is the tangential component of both wavevectors shown in figure 2.5.

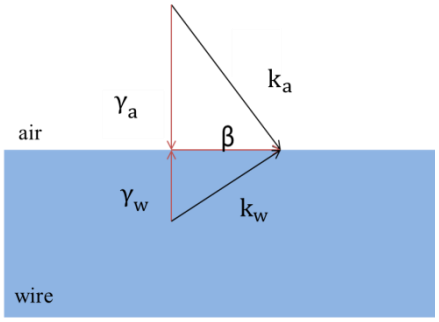

Figure 2.5*: It shows the wavevectors in the NW, k_w and outside, k_a in the air with their vertical, $\gamma_w, \gamma_a$and horizontal components β.Due to boundary conditions the horizontal components for both the wavevectors should be equal in the boundary between the two media.*

From figure 2.5 it becomes obvious that $\beta^2 + \gamma_a^2 = k_a^2$. If $k_a < \beta$ then γ_a is imaginary [11]. The wave function decays exponentially in the radial direction in the air so that the modes are

bound to the wire. If $k_a > \beta$ then γ_a is real and the fields are oscillating in the air which means that there is radiation in the air leaking out from the wire [22]. The conditions for two possible different kind of modes can be summarized by the following conditions

$$k_a < \beta < k_w \text{ bound modes}$$

$$\beta < k_a \qquad \text{leaky modes}$$

In the case of illumination perpendicular to the axis, β=0, the transverse magnetic modes (TM)-electric field parallel to the axis- and transverse electric modes (TE) -magnetic field parallel to the axis- are completely decoupled and only a finite number of them can be excited [21]. More specifically, the larger the radius of the wire the more modes can be coupled to it so more resonances in the absorption and scattered spectra are observed [11, 23]. Except the increase of the number of modes that can be coupled to the NWs, by increasing their radius, their spectral position are shifting. The effective wavelength of coupled light should fit an integer number of times (*s*) in the NW circumference: $\frac{\lambda}{n} = 2s\pi r$, where r is the NW radius. Since s is constant for each mode, an increase in radius causes a red shift in the scattering and absorbed resonances [11, 24].

As it can be seen from figure 2.5, wave vectors β and γ depend on the incidence angle of light. In the case of oblique illumination, hybrid modes EH (non zero electric and magnetic field in the nanowire axis) are excited apart from only TE and TH. As a result, the absorption and scattering efficiencies are angle dependent. This fact is verified from photocurrent experiments of single Ge NWs of 25 nm radius by Cao *et al.* revealing abrupt drop of absorption efficiency at angle of 20° [11]. Moreover, polarization of incident light affects the absorption and scattering of light from NWs. As it is shown from Brönstrup *et al.* [20], for TM polarized incident light the scattering efficiencies are found to be higher than the TE polarized incident light while the absorption efficiencies have the opposite trend. In scattering experiments of individual ZnO nanorods Choi et all also observed higher scattering light intensities of TM polarized incident green laser than TE polarized laser [25]. Furthermore, as it is shown from Brömstrup et al, the resonating wavelengths of scattered light from Si NWs are different for incident light with transverse electric and transverse magnetic polarization [13].

When a light beam strikes the semiconducting nanowires, an electric field is induced inside them. Although eq. (3) and (4) describe the case of static fields, they are also valid for oscillating fields with high frequency, but only if the wire diameter is much smaller than the light wavelength [15]. Consequently, oscillating electric fields appear mainly along the length of the nanowire, which induces an oscillating dipole moment in the same direction. This oscillating dipole moment serves as a source of light with the same frequency as the oscillation frequency and emits mainly the elastically scattered light. Thus, the scattered light has the same wavelength as the incident beam and it is mostly linearly polarized in the same direction as the wire axis. When the diameter becomes larger, scattering from the transverse electric field shows up as reported from Brönstrup *et al.* for Si NWs with 60 nm diameter [13].

2.4 Photoluminescence

Photoluminescence is the radiative recombination of an electron and a hole after their optical excitation. The energy of the emitted photon is equal to the difference of the energy levels. In order that photoluminescence happens, the excitation energy must be higher than the bandgap so that photons can be absorbed. Photoluminescence spectroscopy is a very useful tool for characterising semiconductor materials in terms of their quality, composition and impurity concentrations, depending on the states from which the carriers recombine.

The main transition processes is the recombination of free electrons in the conduction band with free holes in the valence band, and this is the process that dominates in room temperature PL [26]. In order to understand better the room temperature PL spectrum we need to recall the probability distribution of states occupation from carriers given in equations (3) and (4). Since at room temperatures there are carriers in high energy states and energy states close to the conduction band are occupied, the PL spectrum will consist of a peak at energy equals to band gap which will be broadened at higher energies than bandgap energies. At room temperature the bandgap energy can be calculated from Varshni relation (5) [27]:

$$E_g = E_g(0) - \alpha T^2/(\beta + T) \tag{5}$$

$E_g(0)$ is the bandgap band gap at 0 K and α and β are empirical constants depending on the material. For GaAs:

$$E_g(0) = 1.519 \text{ eV}$$

$$\alpha = 5.41 \times 10^{-4} \text{ eV/K}$$

$$\beta = 204 \text{ K}$$

So, at around 40 °C, the band gap energy is $E_g(313 \text{ K}) = 1.4$ eV. From equation (6) [2]:

$$\lambda_g(\mu m) \approx \frac{1.24}{E_g(eV)} \tag{6}$$

We can find that the bandgap energy of 1.4 eV corresponds to wavelength $\lambda_g = 875$ nm.

3 Experimental Details

3.1 Nanowire growth

Our samples are GaAs NWs produced from Aerotaxy. The process starts with the generation of gold NP of the same diameter. For this purpose, gold is evaporated in a high temperature furnace at around 1800℃ and the gold vapors are transferred out of the furnace by a continuous flow of N_2 at 1.5 l/min [28]. Aggregates of various shapes and sizes are formed by cooling down the aerosols and they are transferred to the sintering furnace where at 550℃ they are reshaped into spheres [29]. After this, the aerosol is charged with one electron per particle, and the particles are size selected with the differential mobility analyzer (DMA). The selection of the desired particle size is based on their mobility in the electric field: the mobility is roughly inversely proportional to their diameter [29]. Then the aerosol carried by the N_2 flow enters the growth reactor. In the first stage the temperature of the reactor is at 430℃ and the precursor trimethylgallium (TMGa) is added to the gold particle flow so that an alloy of Ga and Au is formed. In the second temperature zone (550 °C) the precursor AsH_3 is added and the growth is taking place [29]. The aerosol of NWs exits the reactor after it crosses the third temperature zone of 130 ℃ and the NWs are led to the deposition chamber where they are deposited by applying a voltage of 10 kV [28] to a collection plate. In short, the mechanism of the growth is based on the supersaturation of Ga in the alloy of Ga Au particles which initiates the growth by the formation of GaAs crystallite at the surface of the particles [9].

3.2 Experimental set up and experiments

3.2.1 Design of the set up

The purpose of this project is the optical characterization of the aerosol NWs in situ after the growth is completed. Since in the existing process flow the NWs are travelling from the reactor to the deposition chamber through an opaque stainless steel tube, there is no optical access to them. This motivated us to insert an optical cell between growth reactor and deposition chamber to optically interact with the nanowires in motion, as shown in the schematic of aerotaxy, in figure 3.1. The characterisation set-up is physically assembled around this optical cell and placed on an optical bench below the Aerotaxy reactor, as shown in figure 3.2.

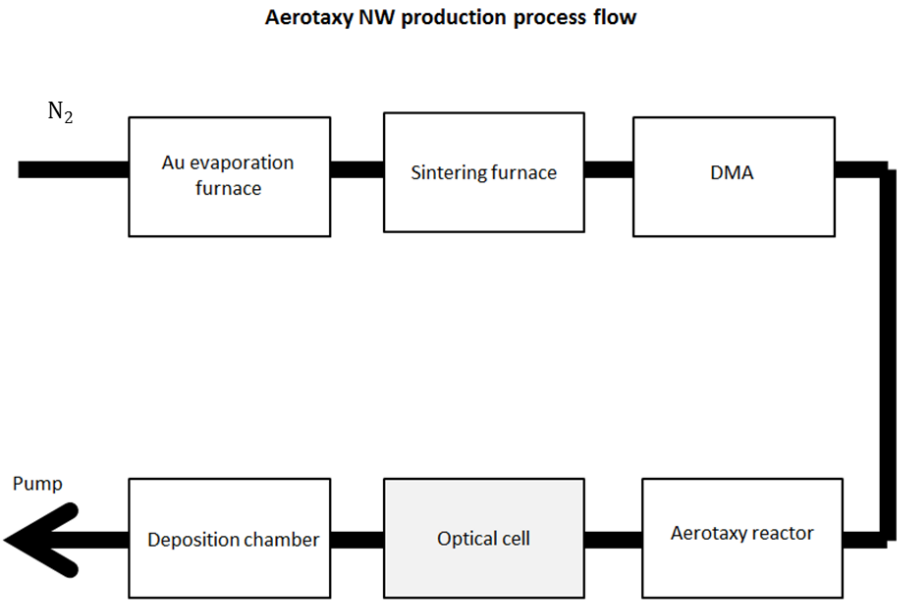

Figure 3.1:*Schematic of Aerotaxy NW production process flow*

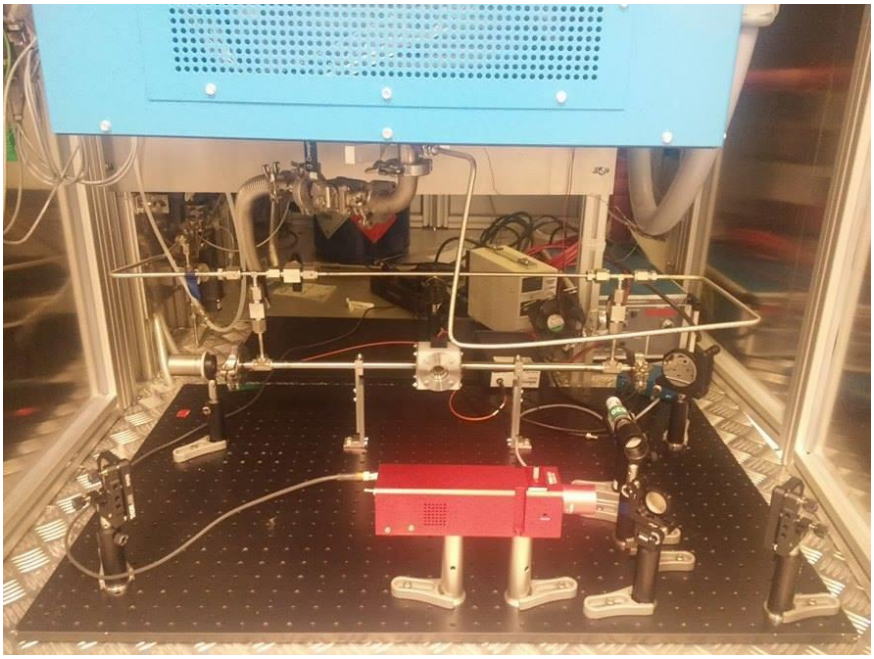

Figure 3.2:*actual picture of the optical characterization set up*

To conduct the optical characterization, namely absorption spectroscopy, scattered light imaging and PL spectroscopy, an alternate stainless steel tube is installed to bypass the regular flow. Using an inlet and outlet valve we can switch the flow between the two lines. Light

from a tungsten halogen lamp or the laser (depending on the experiment), enters the tube, aligned parallel to the flow of the nanowires through one of its windows and, exits from the other end. For absorption spectroscopy the transmitted light collected at this end is coupled to a spectrometer and analysed. For PL spectroscopy and scattered light imaging, laser light source is used and the luminescence signal or the light scattered from the nanowires is captured using the optical cube, placed in the middle of the tube. Parallel plate electrodes are mounted on this cube such that an electric field perpendicular to the direction of the flow of nanowires can be created in the cube. The electric field is used to align the nanowires in the cube, which affects the scattered light escaping from the windows of the cube. For efficiently designing a multitasking apparatus like this, several factors were taken into account. The factors which influenced our design the most, are discussed below.

• **Length of the tube:** Highly sensitive detectors would be required to detect the absorption signal from a few nanowires, therefore the length of the tube, which also serves as the absorption column, should be maximised for pronounced effects.

• **Preserving the laminar flow:** Turbulence in the flow could adversely affect the alignment of the nanowires, when an electric field is applied.

• **Positioning the source and detector:** Optical path for the light outside the tube should be minimized to avoid losses. Even if a collimator is used, light from the lamp is not totally collimated. As a result, the shorter the path the more incident light can be coupled into the tube and more transmitted light can be coupled into the collimator. Since the required strength of the incident source was not known, it was important to limit the losses.

• **Physical constraints due to space.** Due to the limited space available for creating the setup, it was important to optimise the number of components and their positions. While all the components should fit the given space, they should also be easily accessible for allignment and experimental purposes.

Based on the above mentioned parameters, length of the tube was fixed at 60cm. To couple maximum light from the halogen lamp while limiting the turbulence of the flow, the diameter of the tube was fixed at 12 mm.

A common laser source is used for scattered light imaging and PL spectroscopy, to limit the number of optical components. The criteria for choosing the right laser is the wavelength, beam intensity, the size of the profile of the beam and the polarisation of the beam. As it is explained in 2.3.2 in order to excite the charge carriers of a semiconductor, we need energy higher than the band gap energy. So the laser should have shorter wavelength than 875 nm which corresponds to this energy. Furthermore, the intensity of the laser should be high enough so that the excitation is enough for a detectable luminescence signal and detectable scattered light as well. Moreover, the size of the beam profile should be smaller than the tube diameter so that we avoid multiple scattering and minimize background signal. The polarization is an important factor related to the polarizarion dependant imaging. Since we expect highest scattering for polarization of incident light parallel to the electric field lines and minimum perpendicular to them, we need a linearly polarized laser which will be placed

in such a way so that it is at the same time vertically polarized. Ideally, as explained in chapter 2.3.1, scattered light that is horizontally polarized should have zero intensity in the case of complete alignment of the NWs. Unfortunately, because of technical reasons the laser available in the lab was not compatible with these criteria and the Bio ray 520 laser was ordered. Bio ray is a green laser of 520 nm with tuneable beam power up to 50 mW and elliptical beam size of (2.6 x 1.2) mm. It is also linearly polarized - the intensity of the light with polarization along the long axis of the profil of the beam is $2 \cdot 10^3$ times higher than the intensity of the light with polarization along the short axis. To find this number we reduced the output power of the beam to 30 μW by setting the laser controller at 3.7 V and using a filter of optical density 3. The light coming through the polarizer has 23 μW in the vertical direction and 12 nW in the horizontal direction. So this laser definitely fulfils the energy and size criteria and it seems to be sufficient for our first experiments, in terms of intensity (at least for imaging), stability and polarization.

In addition, due to limited space and a need to maximize the length of the tube , different sources and detectors could not be placed in a line. Therefore, mirrors are used to guide the light through a common path for both the laser and lamp, and a flip mirror is used to switch between them as shown in figures 3.3 and 3.4. The mirrors with number (1) and (3) are used for controlling the vertical and horizontal position of the beam and the mirrors (2) and (4) are for controlling the angle of the beam. It is important to control the position and the angle of the beams because these are parameters which determine the efficiency of coupling the light coming out from the tube into the collimator and because we want the laser beam not to strike on the walls of the tube. In this way we tried to optimise and fulfill overall design parameters to create an optical bench. Different experimenst and specific discussion is continued.

3.2.2 Absorption Spectroscopy

For the absorption spectroscopy, a tungsten-halogen light source SLS201 is used. It produces 2799 K blackbody type spectrum with the range of 300 nm to 2600 nm. Since the light of the source is quite divergent and the diameter of the tube is relatively small in comparison with the beam size the collimator SLCS is used which is mounted with threads on the source. A schematic of the absorption spectroscopy set up is given in figure 3.3.

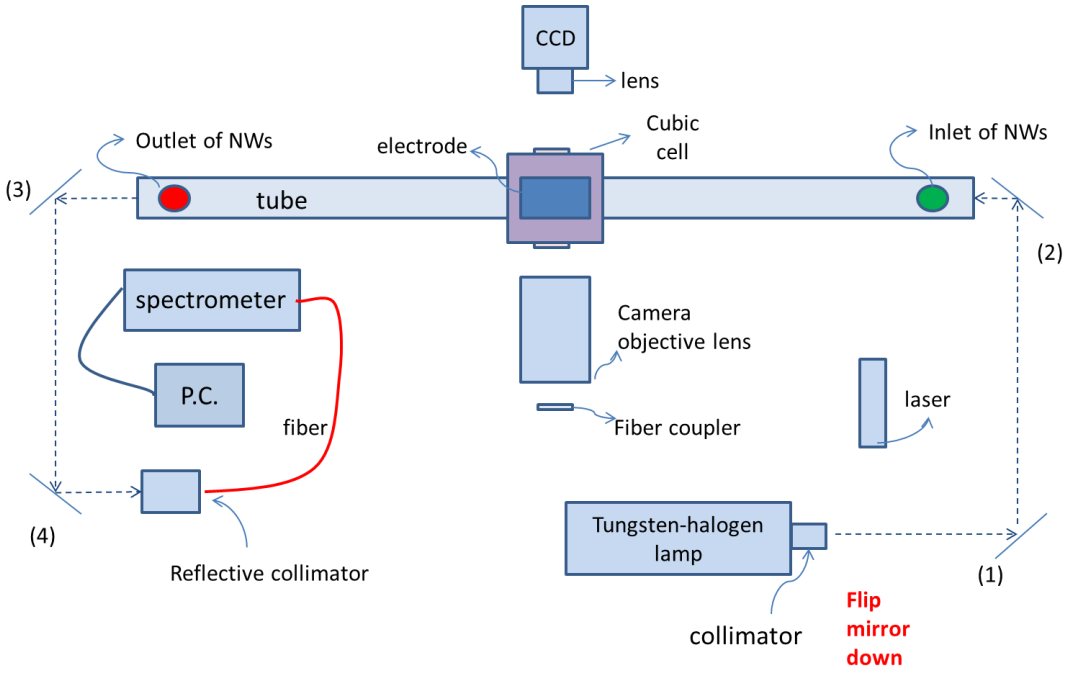

Figure 3.3**:** *The top overview of the set up used for the absorption spectroscopy. The dashed lines show the path of the light. The numbers are for referencing the mirrors*

Having the flip mirror down, the light enters the tube after getting reflected from mirrors 1 and 2, and the transmitted light through the tube is reflected in mirrors 3 and 4 to reach the reflective collimator RC12SMA-P01 which is coupled to the multimode fiber M28L01 of 400 μm. The light is guided by the optical fiber to the fiber spectrometer Avaspec-ULS3648. There it is distributed spatially on a Si CCD array by a grating which consists of 300 lines/nm so that we get the spectrum. Due to space constraints a fiber spectrometer which is small and portable is a good choice to start with the first experiments in the new set up.

Experiments

For the absorption experiments we shined visible-infrared light on randomly oriented nanowires and we detected the transmited light. We expected that reduction of the transmitted signal would show absorption effects. There was no time for conducting rexperiments with aligned nanowires.

3.2.3 Imaging of scattered light

For imaging experiments, a schematic of the set up is given in figure 3.4. A flip mirror is flipped up and the laser beam enters the tube after being reflected from mirrors 2 and 3. The laser light, which is elastically scattered from the NWs and escapes through one of the windows of the cube, is detected for the imaging of the NW flow. The light is captured from the lens and focused on the camera which is placed opposite to the window. The camera used

is a CCD camera since high sensitivity is required for detecting small signal differences in the wavelength of 520 nm, which is the wavelength of the laser. In the case of polarization dependent imaging, a linear polarizer is placed in front of the window.

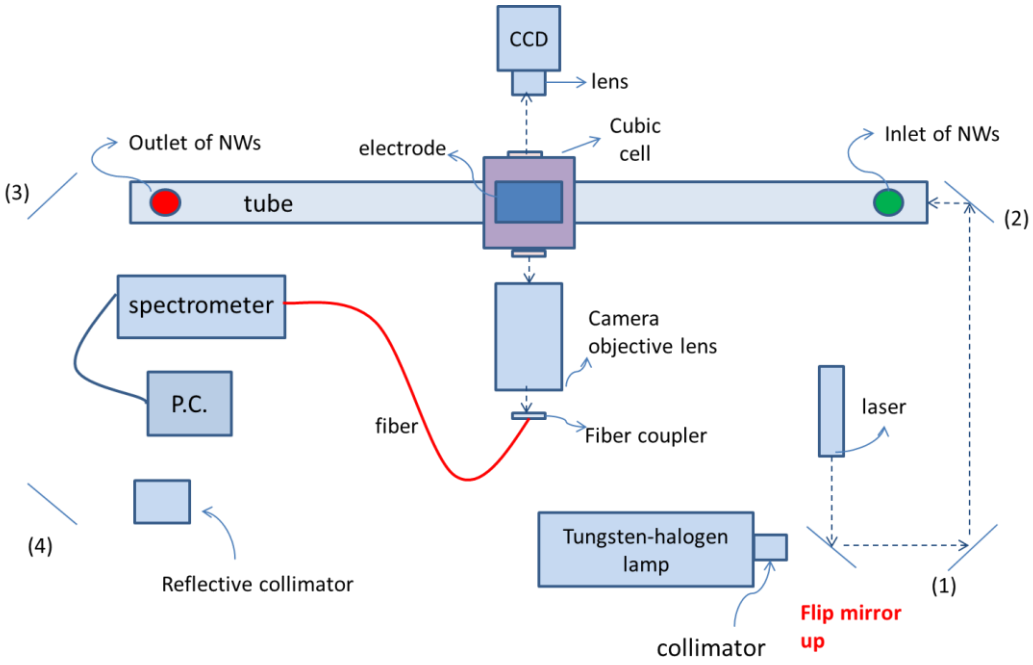

Figure 3.4: *The top overview of the set up used for imaging and PL spectroscopy. The dashed lines show the path of the light. The numbers are for referencing the mirrors.*

Experiments

The average intensity calculated from the scattering images, gives the information about the amount of the material in the tube which can differ because of variations in the number, the thickness and the length of the nanowires. Additionally, the intensity of the polarization selected scattered light depends on the angle of nanowires with respect to the polarization of the incident light. More specifically, in our experiments by applying an electric field we try to align the nanowires vertically - the electric field has vertical direction- and in this case that we expect maximum scattered light with the same polarization as the incident light .

As it is explained in paragraph 3.2.1 the diameter of the NWs is cotrolled from the DMA. Since the magnitude of electric field needed for their alignment depends on the nanowire aspect ratio, in our case it will depend on their length. By increasing the electric field, the degree of alignment increases to the point that the nanowires get completely aligned at a maximum electric field magnitude. Consequently we are expecting that by increasing the applied voltage the polarized selected scattered light with parallel polariazation to the electric field lines will also incease as well as the total scattered light since the laser light is polarized. According to paragraph 2.2 the maximum scattered light will be achieved in different magnitudes of electric field for nanowires with the same diameter but with different length

and will not increase more with furtherr increase of the electric field. So we detected the scatterd light intensity when electric field was applied to the nanowire flow trying to find out which magnitude of electric field correspond to maximum scattered lase intensity. We took videos for different magnitudes of electric field while keeping the set values of growth parameters constant. Unfortunately we did not have the time to conduct the experiment for different set values which determine the nanowire length. Additionally, we detected the scattered light of different polarizations while keeping the applied voltage at 19.7kV and the set growth parameters constant to see how the scattered light intensity is affected.

In all of the scattering experiments we tried to minimize disturbances in the aerosol flow so no deposition or pumping and purging were done during the measurements. In addition, in order to figure out the intensity differencies we processed the data in the way discribed in paragraph 3.3.

During the experiments, some samples were collected and examined later in SEM. The average length of the NWs was (2.3±0.3) μm and their average diameter was (96±11) nm. We can see some of the NWs in the following SEM images.

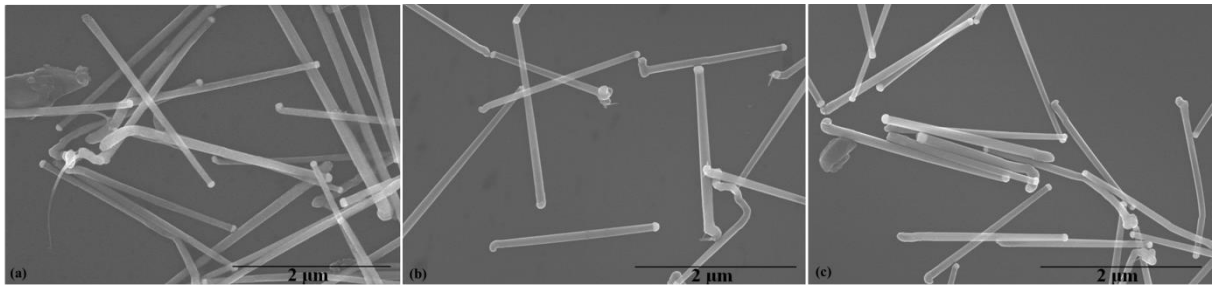

Figure 3.5*: During the running time of thte second and third experiment some NWs were collected and we can see them in pictures (a),(b) and (c). Images courtesy of Sudhakar Sivakumar.*

3.2.4 PL spectroscopy

For PL spectroscopy, as shown in figure 3.4, flip mirror is again flipped up and the laser beam reaches the tube after being reflected from mirrors 2 and 3. The luminescence signal escaping through the other window of the cube is captured by the camera objective lens and focused directly to the fiber. Then the light is guided to the spectrometer for the acquisition of the spectrum. In between the objective lens and the fiber there is a long pass filter which blocks laser light, to avoid saturation of the spectrometer. The same fiber and spectrometer are used here as in the absorption spectroscopy experiments.

The PL set up created for our in situ experiments is quite different from the common PL set ups. The main difference is that because of practical reasons there is no microscope to observe our sample. This makes our task more difficult since we are not able to know with precision from where we are collecting luminescence signal. Therefore, in order to check if our apparatus works many attempts are needed with NWs grown using a recipe which gives good quality defect free NWs.

Due to the fact that we were not able to collect any PL data from the above configuration and that we were restricted from the limited runs of Aerotaxy, we created an additional set up on another optical bench so that we validate the possible errors. The overview of the top view of the auxiliary set up is given in figure 3.6.

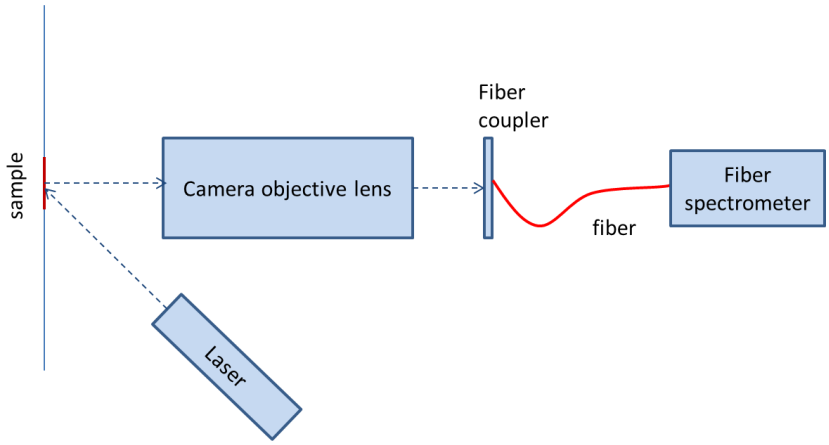

Figure 3.6: *Top view of the auxiliary PL set up with the fiber spectrometer. The path of light is depicted with the dashed lines*

The first check was to confirm that detection of PL signal is possible. For this reason, we used the same laser for excitation and the same configuration for collection and detection of luminescence as in the original set up. Our samples were a GaAs wafer and a sample with Aerotaxy NWs deposited on it. Both of the samples were checked for their luminescence in an already working set up. Since the intensity of luminescence from the wafer was expected to be much higher than the luminescence from the NWs, the wafer was used first to optimize our configuration, changing the distances between the components and the focus of the objective. For the conditions of maximum signal from the wafer we investigated the NWs from which unfortunately there was no detectable signal. Consequently, this led us to combine our auxiliary set up with an already existing set up as. What we did this time was to keep everything the same except the detection part. To do so, the end of the fiber which was coupled to the fiber spectrometer was coupled in this case to a fiber collimator and the collimated out-coming light was directed to the other set up ending up to the spectrometer SPEX270M. The top overview of the last created set up is give in the figure 3.7

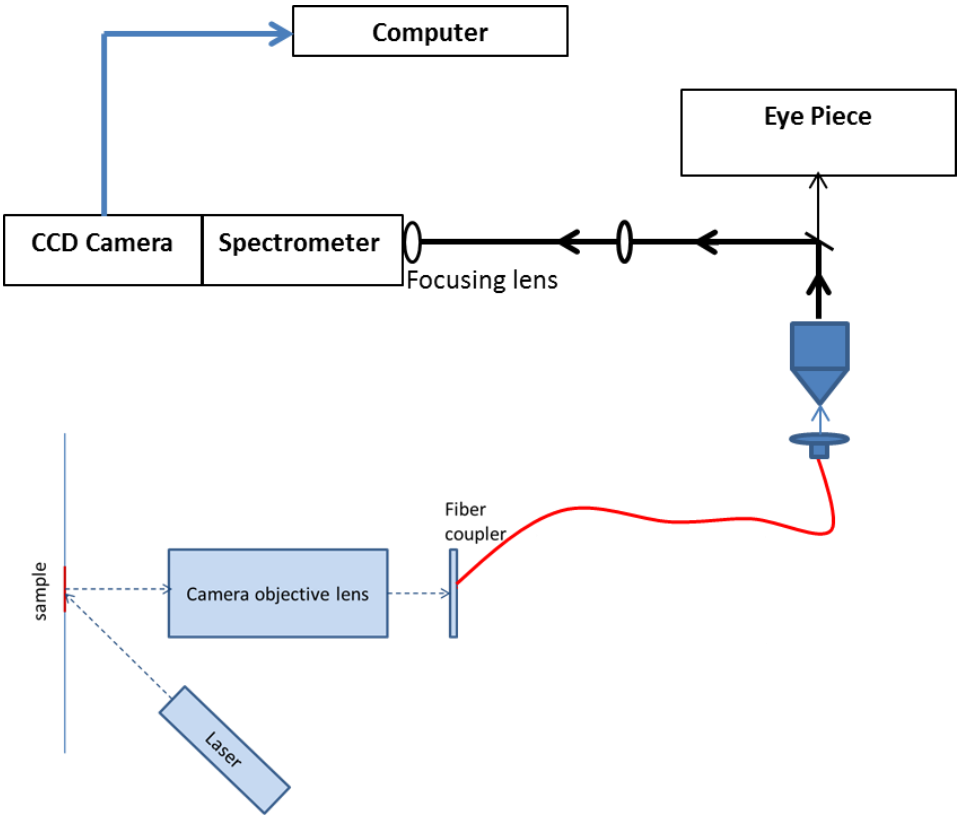

Figure 3.7:*Auxiliart set up with the the spectrometer SPEX270M*

3.3 Processing of data

In order to find out the differences in the intensity of the scattered light from the imaging of the flow, we recorded a short video of it. From this video we extracted the frames and we cropped from each frame the area that we wanted to use, as shown in figure 3.8. Then we added the intensity values of each crop and we got one sum value for each frame. In total, we had as many sums as the number of frames that the video consisted of. Finally, we averaged these sums and the value that we got represents the intensity. We call these numbers average intensities. We did this procedure for three different crops as shown in figure 3.8 with the orthogonals of different colours. The reason for this is that in the edges of the electrode, the electric field lines become curved so we may have differencies in the signal depending on NW alignment. The extraction of the frames from the video and the sums were done in MATLAB with a script written for this purpose.

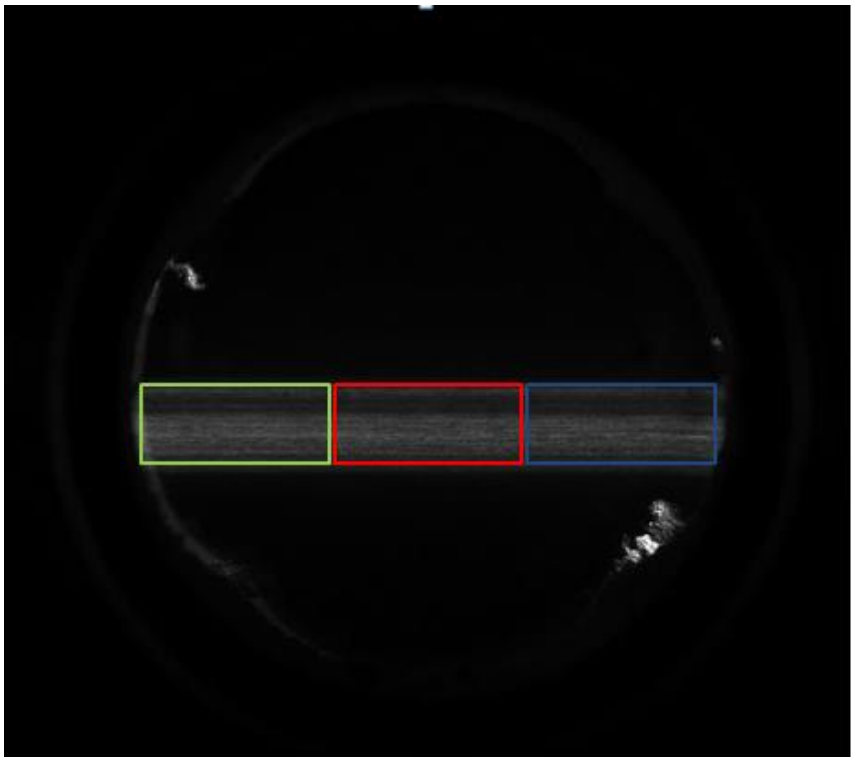

Figure 3.8: *In this picture we can see the flow from NWs by imaging the scattered light. The three rectanglse of equal size show the crops from which we derived the average intensities. In the restuls section, green = 1st crop, red = 2nd crop and blue = 3rd crop.*

3.4 Calculations

The difference in the energy of a NW because of rotation from angle θ to an angle 0° with respect to the electric field lines is calculated using equation (5) and it is given from equation (7):

$$W(E,\theta) = \Phi(E,\theta) - \Phi(E,0) = \frac{1}{2}(2\pi\varepsilon_o)VE^2\left[\frac{\cos^2\theta+1}{1/(\varepsilon-1)+k_1} + \frac{\sin^2\theta}{1/(\varepsilon-1)+k_2}\right] \quad (7)$$

In figure 3.9 we plot $W(E,\theta)/kT$ vs the angle, θ, for electric field $E = 9\cdot10^5$ V/m, which is the magnitude of the energy lost from rotation relative to the Brownian energy. This electric field corresponds to the electric field in the center of our cube when we apply a voltage of 20 kV in our experiment.

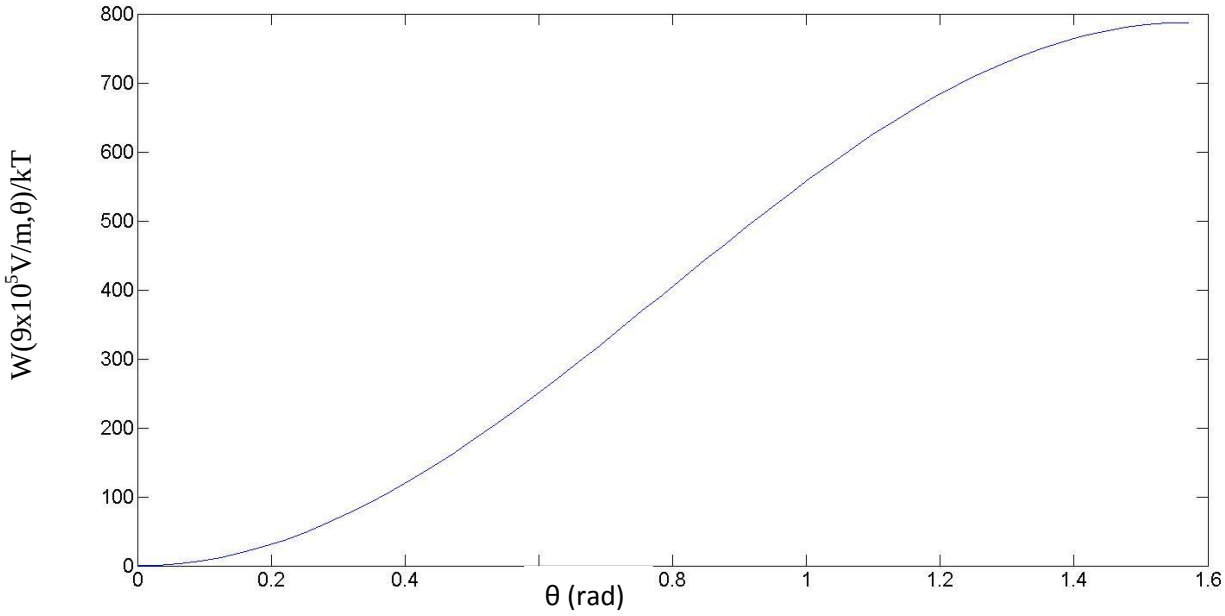

Figure 3.9: *Energy gained from a NW which is in the center of the cubic cells when it rotates from angle θ to angle 0° parallel to the elctric field lines.This is for the case when the electric field in the center of the optical cell is* $9 \times 10^9\ V/m$

According to Fuchs [14] and if we have laminar flow of NWs in the tube, we should be able to align the NWs because *W/kT* for θ=0 is one order of magnitude higher than the minimum value that he proposes.

4 Results and discussion

4.1 Overview of Aerotaxy nanowire growth results

Aerotaxy is an under development tool for production of nanowries at commercial scale. Its capability to produce nanowires in air is unique but also adds certain challenges. While the possibility of producing good quality nanowires has been demonstrated, it is difficult to consistently maintain that quality over time. The nanowires produced are often plagued with the high standard deviation in the length of different nanowires, initiation defects, kinks etc. Moreover, Aerotaxy reactor degrades with time due to depositions on its walls and cloggings in the injectors, which decrease the throughput of the nanowires and degrades its quality with time. There are constant variation in their length and diameter in the range of 10% to15%. In short, this implies that the nanowires characteristics, such as their length and quality, are time dependent and this directly reflects in the inconsistency of some of the in situ characterization experiments.

4.2 Imaging of scattered light

4.2.1 Imaging of scattered light without applied Electric field

In order to find out the correlation of the size and concentration of the particles or nanowires on the scattered laser light intensity and to define a baseline, we performed an experiment to compare the scattering from the nanoparticles and nanowires with different diameters and concentration. We compared the scattering from nanoparticles with 40nm and 80nm diameter and nanowires grown from these seed particles, in different experiments. The nanowires and particles with these diameters were grown for 2 different concentrations: $3.5 \cdot 10^{-5}$ cm^{-3} and $8.5 \cdot 10^{5}$ cm^{-3}. For comparison, figure 4.1 gives the scattering image of NW flow with smallest diameter and lowest concentration, largest diameter and highest concentration and the flow of NP with 80 nm and the highest concentration of $8.5 \cdot 10^{5}$ cm^{-3}.

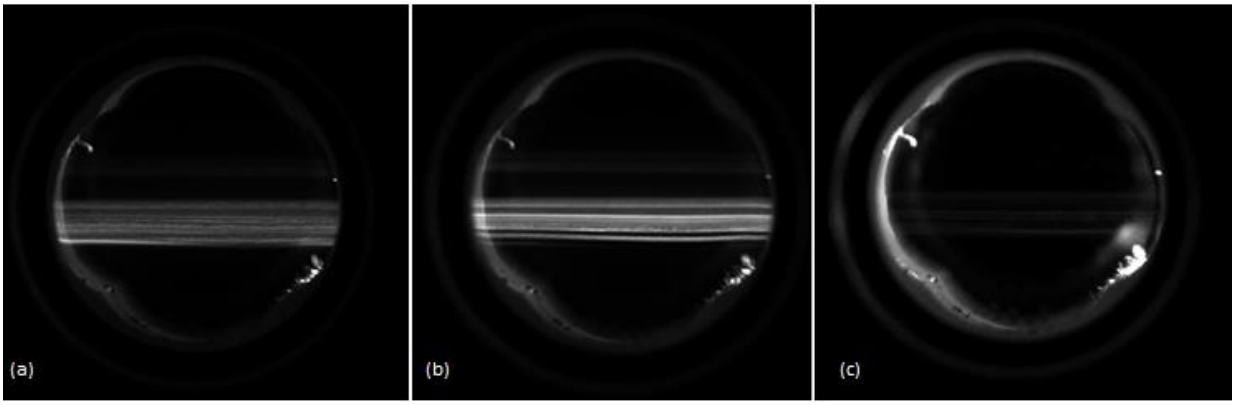

Figure 4.1: *(a) shows the scattered light from the flow of 40 nm NWs with concentration of $3.5 \cdot 10^{-5}$ cm^{-3}. (b) shows the scattered light from the flow of 80 nm NWs with concentration of $8.5 \cdot 10^{5}$ cm^{-3} (c) shows the scattered light from the flow of 80 nm Au NPs with concentration $8.5 \cdot 10^{5}$ cm^{-3}. The laser power is at 50mW and the image is contrsast and brightness enhanced so that the flow is visible.*

The scattered intensity from the NPs was so low that it was barely detected by the camera, and that too only for 80 nm gold particles and set value of flow concentration at $8.5 \cdot 10^{5}$ cm^{-3} at maximum laser intensity. Figure 4.1(c) gives the image captured by the CCD in this case. Although we have maximum laser power, the image needed to be post processed to enhance the contrast and the brightness so that the low signal becomes more visible. For lower flow concentration of nanoparticles or smaller diameter, no signal was collected by the CCD even at maximum laser intensity. Whereas the nanowires were easily detectable and the scattered light images of the nanowire flow are given in figure 4.1(a) and (b).In these figures we can see that scattered intensity is higher for higher density and bigger diameter of nanowires as it is expected.

In fact, this experiment was used in an occasion to discover an obstruction in the nanowire growth due to depletion of the precursor – TMGa – flow. Therefore, it was successfully used to provide an immediate feedback of the growth parameters, which is an expected outcome from in situ characterization techniques.

4.2.2 Imaging of scattered light with applied Electric field

Imaging of nanowire flow from unpolarized scattered laser light

In this experiment, the vertically polarized laser beam was sent through the flow and voltage up to 6.5 kV was applied to the cubic cell. The scattered light was detected from the camera.

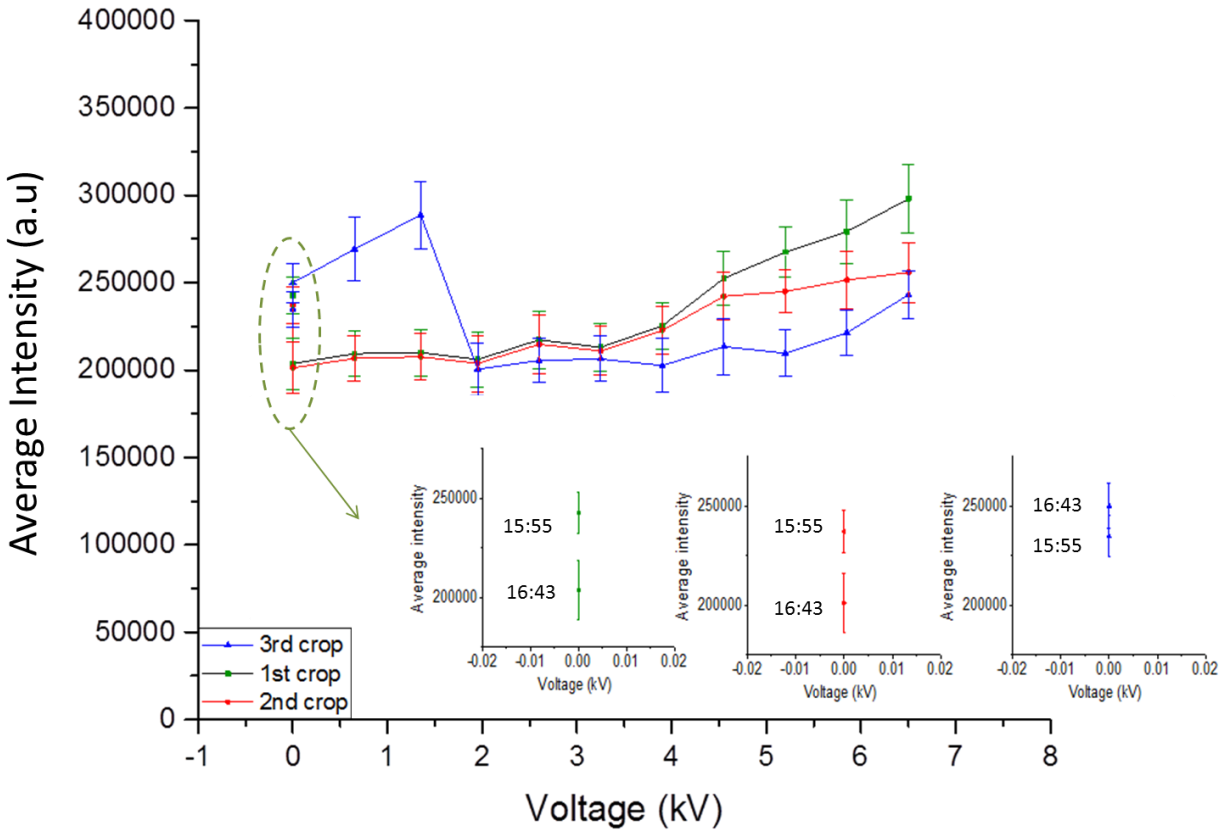

Figure 4.2: *This figure shows the average intensities of the three crops at different applied voltages.Two measurements have been done at zero applied voltage, one in the beginning and the other one in the end of the experiment. These values can be seen in the inset of the figure.*

In figure 4.2 we can see the average intensities with their standard deviations for the three different crops, as discussed in section 3.3. The scattered light in this experiment is not polarization selected. The whole experiment lasted for 50 minutes and the average intensities at 0 kV were measured twice, once in the beginning and once in the end of the experiment so that we check the stability of the flow through time. We can see better the zero electric field intensities at different times in the inset of figure 4.2. As we can see, the scattered light is reduced in the end of the experiment for the first and the second crop which could mean decrease in the concentration of NWs, in their length or in their diameter. Despite the decrease of signal through time there is an increasing trend in the intensities of the first two crops and in the third one after 1.51kV. Table 1(a) gives the difference in the signal intensity in terms of percentage between the start and in the end of the experiment and table 1 (b) gives the difference in signal because of the electric field.

	Difference between the start and the end of the experiment in the signal intensity
First crop	-16%
Second crop	-15%
Third crop	+6%

(a)

	Difference in the signal intensity between the case 6.5kV and 0kV
First crop	+ 46%
Second crop	+27%
Third crop	+3%

(b)

Table 1(a)*The table gives the difference in signal intensity between the start and the end of the experiment.We see a decrease in the scattered light for the first two crops and a slight increase in the third one which is in the error limit.****(b)****The table gives the increase in the signal for all the crops when there is voltage compared to the case without voltage.*

In all of the crops the signal seems to increase at higher bias as expected. Since the intensity of the scattered light does not saturate we proceed to the next experiment where we apply higher voltages for aligning the nanowires.

Imaging of nanowire flow from polarization selected scattered laser light

In this experiment we applied electric field to the flow with maximum value at 19.7kV and by placing the polarizer in front of the window of the cube we detected the horizontally polarized scattered light. Every time, before moving to the next step of voltage, we measured the scattered intensity without electric field so that we know if the nanowire flow changes with time. The results are given in figure 4.3.

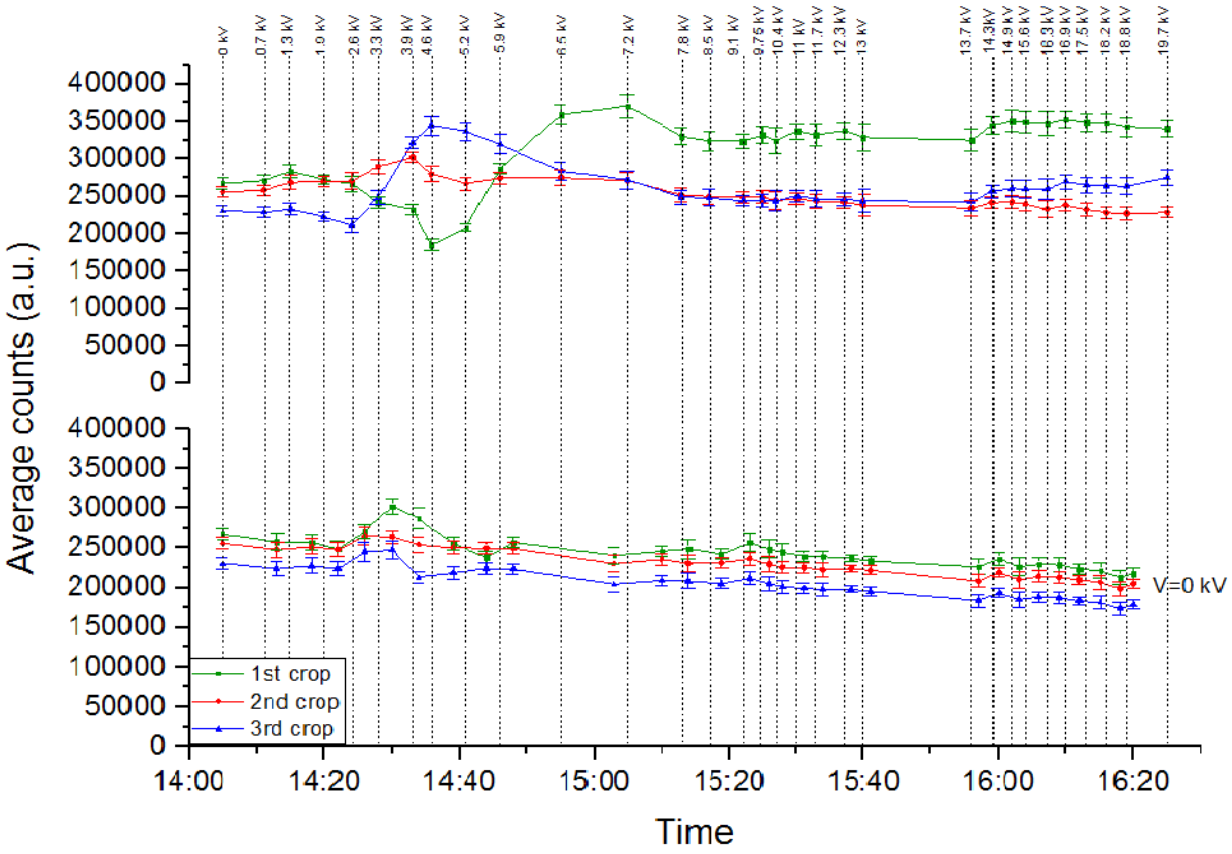

***Figure 4.3**: In the figure we see two different sets of plots. The upper one shows the average intensity of the horizontally polarized light at different applied voltages, I_V, which are given on the top, for the three different crops. The time that these measurements took place is given in the x axis. The low set of plots gives horizontally polarized signal for the three different crops at different times and without the application of electric field, I_0.*

In figure 4.3 we see two different sets of plots. In the upper set we see three plots with the average intensities of the signal of the three different crops at different voltages (given on the top of the figure) and different times (given in the x axis). In the three lower plots we see how signal changes through time at zero electric field. We notice that there is a decreasing trend in the scattered signal for all the crops when we do not apply voltage. This trend could be a result of a decrease in the concentration of NWs in the flow or a decrease in the NW length or diameter as we have already mentioned. To remove the incosistency on nanowire characterisitcs and nanowire flow, which can affect the intensity of the scattered light along with electric field, we plot $I_V - I_0/I_0$ vs the applied voltage, where I_0 is the intensity of scattered light without voltage taken just before the intensity with V volts: I_V. The results are given in figure 4.4.

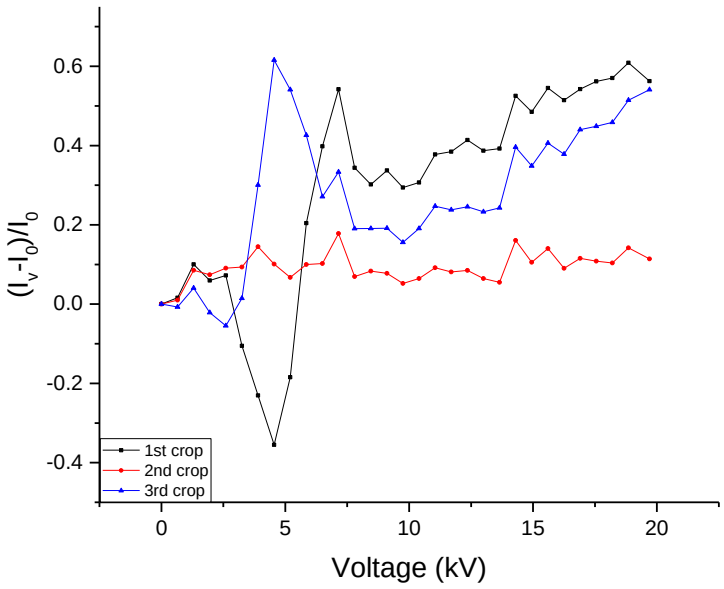

Figure 4.4: $\frac{I_V - I_0}{I_0}$ *vs the wavelenth where* $\boldsymbol{I_0}$ *the intensity of scattered light without electric field taken just before before the intensity with V volts:* $\boldsymbol{I_V}$.

Figure 4.4 shows that the horizontally polarized scattered light is increasing with electric field in the first and third crop after 9 kV while it remains almost steady in the second one. This is contrary to what we would expect theoretically.The laser that we use is vertically polarized such that, ideally the nanowire axis, laser polarization and the electric field lines are in same direction as shown in figure 4.4. Theoretically, according to section 2.3.1, the nanowires in the flow should scatter light only with polarization parallel to their axis, while scattered light with horizontal polarization should be zero. Practically, in experiments, scattered light with horizontal polarization cannot be zero because as we move out from the centre of the cube the electric field becomes more curved. In figure 4.4 we can see the electric field lines and the nanowires if the electrodes would form an ideal plate capacitor which develops strong enough electric field to align the nanowires. In figure 4.5 we can see the simulated electric field in the cube which differs from that of the ideal capacitor. Consequently not all of the nanowires will be vertically aligned even if the magnitude of the field is big enough.

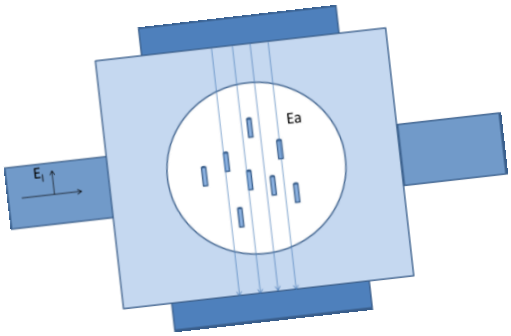

Figure 4.5: *The schematic of the inspection cube through which the scattered light is imaged when NWs are alligned vertically and are illuminated with the perpendicularly polarizes laser beam*

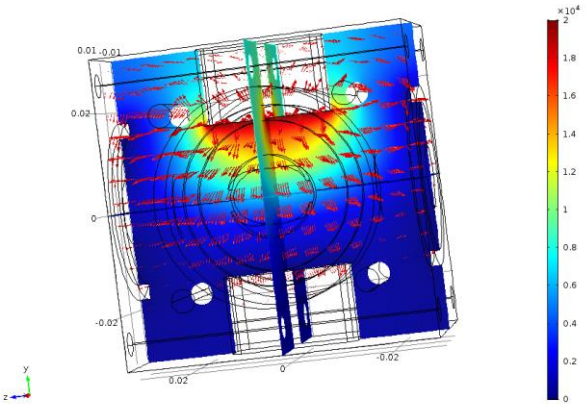

Figure 4.6:*Electric feild distribution in the cubic cell when voltage of 19.7 kV is applied*

As mentioned in paragraph 2.3.1 the horizontally polarized signal is supposed to decrease with increasing electric field to zero level when NWs are completely aligned. Especially in the second crop where electric field lines are more vertical we would expect a decrease in the signal which is not the case here. On the other hand as we move out from the center of the cube where electric field lines are more curved we expect non zero value horizontal component of polarization. In our case this component is about two times higher when maximum voltage is applied compared to the case when no voltage is applied. This fact is a sign that the applied voltage has an impact in the direction of nanowires but more experiment are needed so that we draw a more specific conclusion. So we proceed to the next experiment.

Imaging of nanowire flow with scattered light of different polarization at maximum applied voltage

In this experiment we kept the voltage at maximum value 19.7 kV and we measeuresd the average intensities of different polarizations of the scattered light. An angle equal to 0° corresponds to scattered light with polarization parallel to the electric field and and angle equal to 90° corresponds to horizontally polarized light, perpenducular to the electric field in the cube. The results are given in figure 4.6.

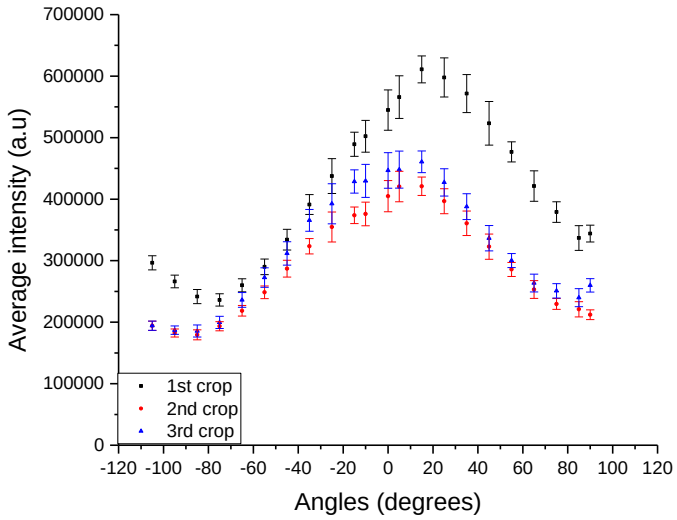

Figure 4.6: *Polarization dependent detection of elastically scattered laser light for an applied voltage of 19.7 kV.*

As we can see, the signal is maximum at around θ=0° and minimum at around θ=90° for the second and third crop while it is a bit shifted for the first crop. Ideally, in the case of alignment, the intensity of transmitted light through the polarizer should follow Malus's law: $I = I_o \cos^2(\theta)$ [26] which implies zero intensity at $\theta=90^0$. It would be difficult to achieve complete alignment in our case and consequently zero scattered signal with horizontal polarization so, a possible explanation of figure 4.6 could be that the nanowires are partly aligned. Considering now that the maximum intensity of the three different crops is about 60% higher than the lowest and taking into account that the laser is vertically polarized, we could say that 40% of the laser beam is randomized in terms of polarization due to randomly oriented nanowires. To the contrary, in the previous experiment, the fact that the first and the third crops have similar trend when electric field is increasing, show an effect of the electric field on the direction of the nanowires in the flow. Therefore it is hard to draw any firm conclusion.

4.3 Absorption spectroscopy

To investigate the absorption from NWs we conducted experiments with three different diameters and two different aerosol concentrations C. Since the NWs have a gold particle on the top which may affect our spectra, we conducted absorption experiments with Au NPs of the same aerosol concentrations and diameters as we did with the NWs. The results are given in the figures 4.7, 4.8, 4.9 and 4.10. Each direct spectrum that we took was an average of 6000 spectra with integration time of 400 μs for each one.

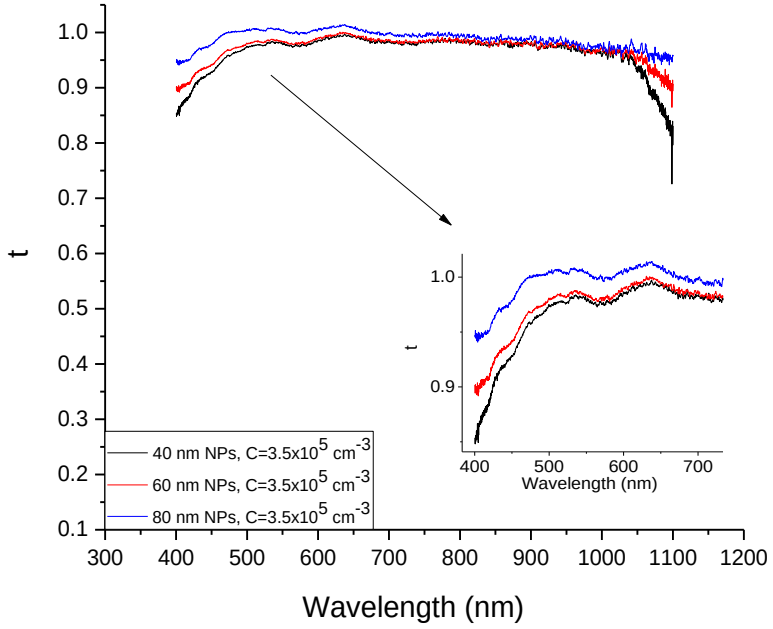

Figure 4.7: *Light absorption spectra for "low" concentration particless .t is the relative light intensity defined as* $\boldsymbol{t = \frac{I}{I_o}}$*, where I is the intensity when there are NPs in the flow and* $\boldsymbol{I_o}$ *is the intensity of light when there is only Nitrogen in the tube. The figure shows the transmitted light relative intensity for 3 different diameters of NPs with the same concentration in the aerosol flow. The inset shows better the features in small wavelengths*

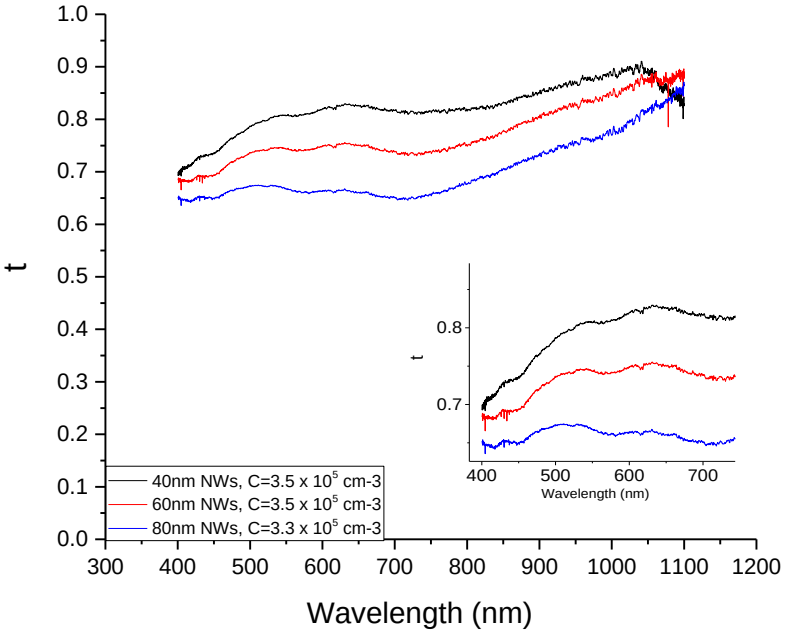

Figure 4.8: *Light absorption spectra for "low" concentration wires.t is the relative light intensity defineds as* $\boldsymbol{t = \frac{I}{I_o}}$*, where I is the intensity when there are NW in the flow and* $\boldsymbol{I_o}$ *is the intensity of light when there is only Nitrogen in the tube. The figure shows the relative light intensity for 3 different diameters of NWs at the same concentration with NPs in the aerosol flow given in figure 4.6. The inset shows better the features in small wavelengths*

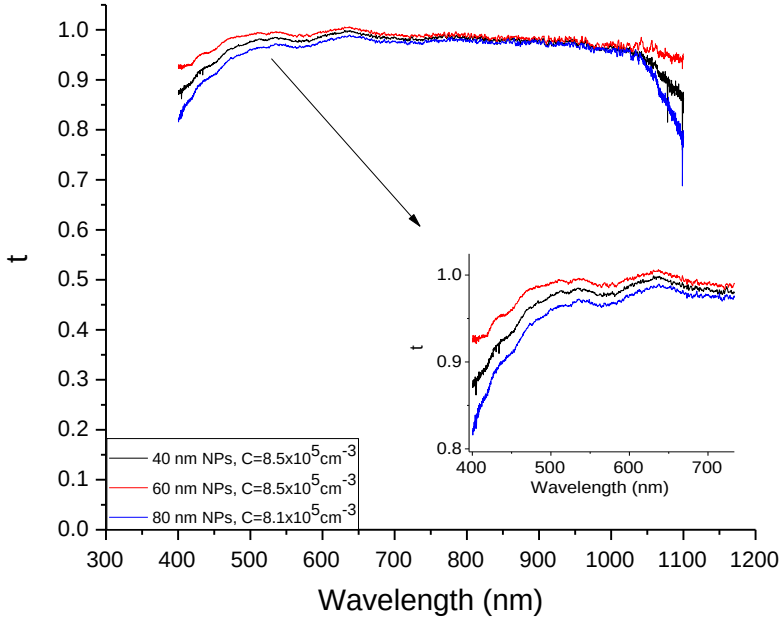

***Figure 4.9**: Light absorption spectra for "high" concentration particles and wires. See figure 4.6 for further details*

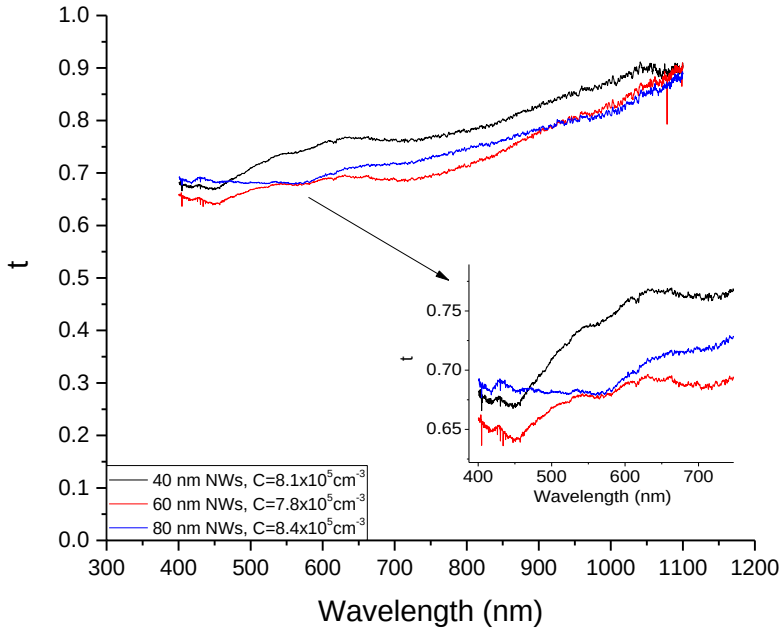

***Figure 4.10:** Light absorption spectra for "high" concentration particles and wires. See figure 4.7 for further details.*

In the above figures t is the relative intensity and it is given by $t = \frac{I}{I_o}$ where I is the transmitted light intensity either with Au NPs or with GaAs NWs in the tube, while I_o is light intensity when there is only flow of Nitrogen in the pipe. We call I_o as the reference. Figures

4.8 and 4.10 show that attenuation from NWs is more significant than the attenuation from the NPs. This is expected since the light is interacting with more matter. Figure 4.7 and 4.8 show that when the size and the concentration of Au particles and NWs in the flow increased, the transmission signal decreased which is also expected. To the contrary, we see in figures 4.9 and 4.10 that this was not the case for the experiments with high concentrations of aerosol particles. Fast change in the parameters controlling the diameter may result in a flow with an extended range of diameters which may be the source of the error. Therefore, we will exclude from any discussion the nanoparticles and nanowires with high concentrations in the flow. Unfortunately, due to technical problems of Aerotaxy tool we could not repeat these experiments.

In figure 4.7 we can see that t is very high for the Au particles – almost all the light is transmitted. In figures 4.7 and 4.8 we see that in the visible range, structures appear in the spectra of both Au particles and NWs which are quite similar. To check the source of these structures we plot $\frac{(t)_{NWs}}{(t)_{NPs}}$ vs the wavelength for low densities of aerosols. This quantity from now on will be called *fraction*. The fraction and the relative intensity for low concentration of NPs and NWs are plotted together in the figure 4.11.

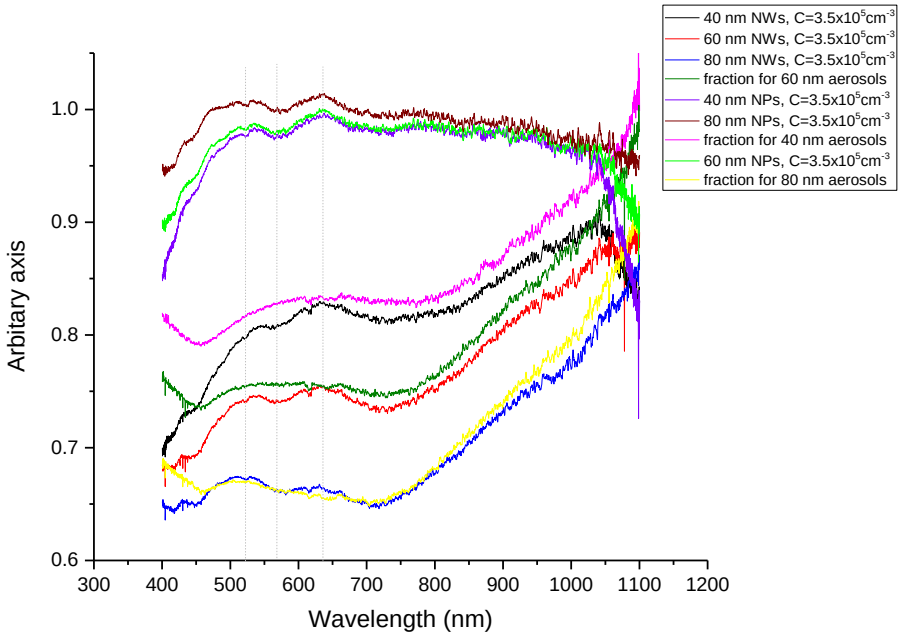

Figure 4.11:*The figure shows the a for NWs and NPs for low concentation and the fraction.*

In figure 4.11 we can see that the structures in the visible range mostly smoothen out, which could probably mean that they are related to Au NPs. Au particles have a plasmonic resonance at around 520 nm for diameters larger than 20 nm, and the peak shifts as their size increases [30]. The plasmonic resonances affect both absorption and scattering [30]. If the size of the particles is small, attenuation is mostly because of absorption, but as the size

increases, scattering dominates [30]. So, one probable explanation could be that the dip in the plots appears because of absorption due to surface plasmonic resonances of Au. But we can see also that the dips do not shift as the particle size increases and that there are structures which do not correspond to the plasmonic resonance of gold. The absence of a shift in the spectral dips could be due to the fact that the size selection is not 100% precise and that there are particles with a range of diameters.

Moreover we can see that for wavelengths longer than about 750 nm, the transmission of light for NWs increases and there is almost no change in this spectral region after taking the spectral ratio. The attenuation starts to increase at shorter wavelength or higher energies than the bandgap so, we could probably say that the effect of attenuation is because of absorption. At the same time, at shorter wavelengths scattering is also enhanced, so certain conclusion can be drawn. Additionally, the absorption edge corresponding to the band gap is not distinguishable from the overall slope of the curve.

Furthermore, no absorption or scattering resonances are observed. Incident light is unpolarized and since the NWs are randomly oriented, we would expect that the different dips in the graph due to higher absorption will smear into each other, this doesn't seem to happen in our case. Resonances are very sensitive to dimensions and consequently to shape. NWs grown from Aerotaxy do not have the perfect ideal nanorod shape which may be the reasons why we do not observe any smearing of resonances. Due to time limitation absorption spectroscopy to aligned nanowires was not conducted.

In addition to above experiment, a stability check for the source was conducted to identify experimental errors. Spectra were taken at different times t during the same day starting from $t_1 = 10{:}52$. The ratio: $I_t/I_{10:52}$ vs the wavelength is plotted and given in figure 4.12.

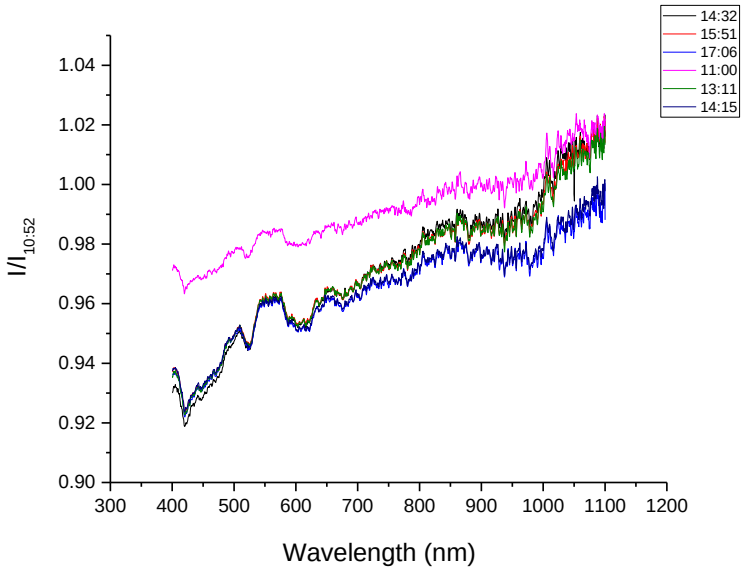

Figure 4.12:*The figure shows the intensity ratio* $\boldsymbol{I_t/I_{10:52}}$ *vs the wavelength, where* $\boldsymbol{I_t}$ *is the transmitted intensity through the tube at time shown in the inset of the figure and* $\boldsymbol{I_{10:52}}$ *is the tranmitted intensity through the empty tube at 10:52.*

Since our experiments last up to five hours, any dips in our plots with magnitude smaller than 0.1 probably were affected also from the source fluctuations. The source fluctuations are comparable in magnitude with the dips in the transmission spectra of Au particles which we should not neglect.

4.4 PL spectroscopy

Below, in figure 4.13 we see the PL signal from a GaAs wafer taken with two different spectrometers: the fiber spectrometer ULS3648 used in the Aerotaxy set-up and the SPEX270M spectrometer. To record the spectra, the light captured by the objective lens was coupled to the fiber. In figure 4.13 we see the spectra of both the GaAs wafer and GaAs NWs using the SPEX270M.

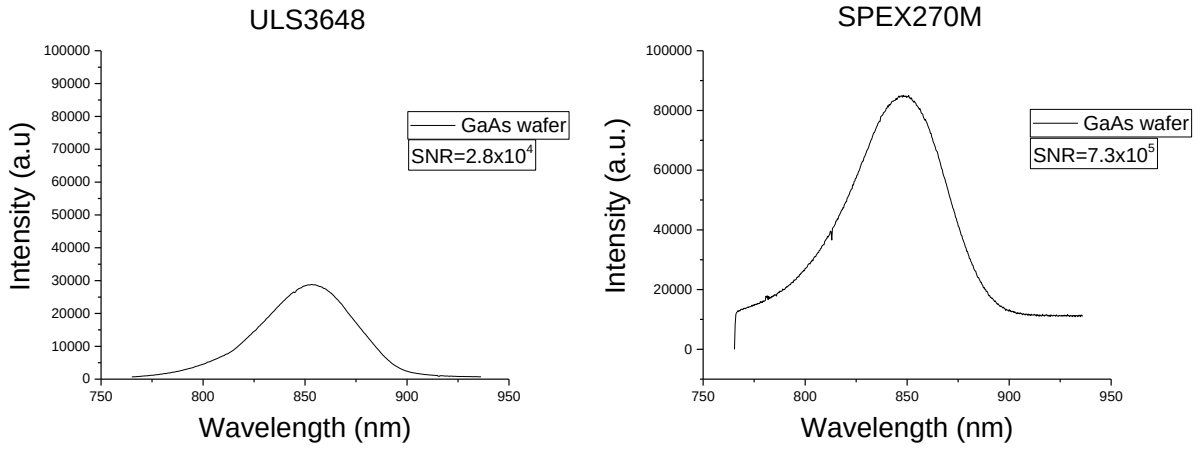

(a) (b)

Figure 4.13:(a) *PL signal from GaAs wafer using the fiber spectrometer* ***(b)****PL signal from the GaAs wafer using the spectrometer SPEX270M.*

The integration time for the wafer was 10 seconds and for the NWs 2000 seconds, but we compensated for the difference by dividing the direct spectrum from NWs with a factor of 200. We notice that the SPEX270M is more efficient as it has better signal to noise ratio (SNR).

In figure 4.14 we see the Pl spectrum from the GaAs wafer and the GaAs Aerotaxy nanowires taken with SPEX270M.

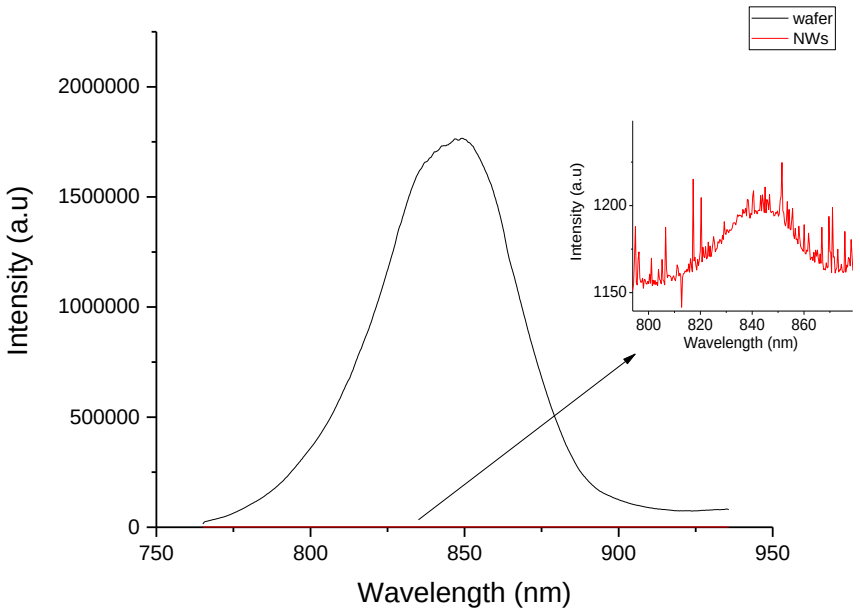

Figure 4.14 *This figure shows The PL signal from the wafer (black) and the PL signal from the NW sample UE3892 (red).In the inset we can see better the PL peak which is comparable to the noise level.*

The difference in the signal intensity coming from the wafer in figures 4.13 (b) and 4.14 is due to the fact that better focus was achieved in the second case. Looking at figure 4.14 we see that the PL signal of NWs is extremely low even by using SPEX270M which is more efficient. As a result the detection of the PL signal with the use of the fiber spectrometer, which is less efficient, seems difficult.

One of the possible reasons for low efficiency of fiber spectrometer, which affects PL signal from NWs is the slit size. In all the spectra taken with SPEX270M, the slit width was adjusted at 7 mm and so all the collected light from the fiber reached the CCD detector. In the case of fiber spectrometer, the maximum slit width is 25 microns which means that the light reaching the CCD detector of the spectrometer is only a part of the light collected from the fiber. The profile of the beam light coming out from the fiber has a surface area of $\pi \cdot r^2 = \pi \cdot (200\ \mu m)^2 = 125664\ \mu m^2$, where r = 200μm is the diameter of the fiber. Roughly the maximum light that the slit can ´´see`` is $(400 \cdot 25)\ \mu m^2 = 10000\ \mu m^2$, which means that only 8% of the light collected from the fiber is detected by the CCD. Furthermore, there is a difference in the CCD detector of the two different spectrometers. SPEX270M has a back thinned CCD chip which has higher quantum efficiency than a simple CCD which is used in the fiber spectrometer. At 600 nm SPXS270M has QE=85% and the fiber spectrometer has only 40% which is very low. We could compensate for these losses by increasing the integration time in the fiber spectrometer but integration time higher than 35 seconds was saturating the CCD chip, due to high thermal noises or dark current. The CCD of the SPEX270M is nitrogen cooled to -133˚which decreases the dark current and enables more efficient detection of low signals than a simple CCD.

Despite all the advantages of SPEX270M, the PL spectra shows a poor signal to noise ratio, when the luminescence is transmitted using a fiber, the maximum transmitted signal restricted by the numerical aperture of the fiber. Room temperature PL spectra acquired without using a fiber coupled transmission, in figure 4.15, confirms the same.

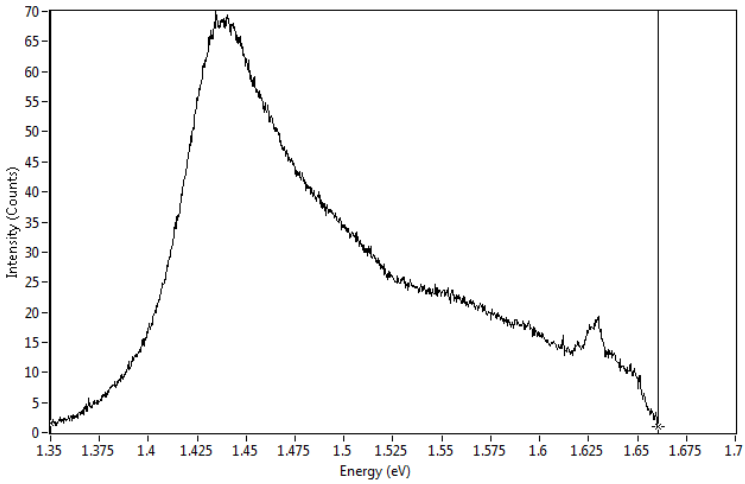

Figure 4.15:*Room temperature PL of the GaAs NWs sample*

5 Conclusions

The aim of this thesis was to perform in-situ spectroscopic studies, namely absorption, scattering and PL, of the Aerotaxy nanowires. Designing a universal optical setup to perform all three studies was challenging in itself. This was further complicated by the fact that it had to be installed, for in-situ measurements, in the space available next to the already existing Aerotaxy setup. Within the limitations of the thesis, we designed and assembled a setup which could ideally perform all the three different studies.

Imaging from laser scattering can be used to find differences in the concentration of NWs in the flow but real time estimations of scattered intensity, needs processing of data to be programmed in a more advanced way. Despite the fact that according to theory the applied electric field was more than enough for aligning the NWs, it is hard to draw any conclusions from the conducted experiments except that the electric field had an impact on the direction of the wires. We should also take into consideration that turbulence in the flow and not perfectly straight nanowires could have affected negatively the results. Since the number of the experiments is small, more experiments need to be done so that we draw solid conclusions. One of them could be to repeat the imaging of nanowire flow with scattered light of different polarization but this time at zero applied voltage and compare the results with the case when we have maximum applied voltage. We could also repeat the second experiment of imaging, but detect the vertically polarized light. In addition, we could repeat all the previous experiments with higher electric fields.

Absorption spectroscopy showed that the effect of Au NPs in the absorption is very close to the effect of the intensity fluctuations of the light source so it is hard to draw conclusions. From the results for NWs, we can see that attenuation of light is proportional to the diameter and the concentration of the NWs in the tube. No information about their quality or diameter can be derived. A simulation study along with more experiment is recommended.

In situ PL spectroscopy was not achieved and the experiments with the auxiliary set-up point to the issues that that we faced. We investigated the performance of the fiber spectrometer by comparing the luminescence signal of a high quality GaAs wafer detected by the fiber spectrometer with the PL signal detected by a conventional spectrometer. Collection efficiency found to be very low because it is limited from the numerical aperture of the fiber and the slit of the fiber spectrometer. These factors in combination with low quantum efficiency and high dark current because of absence of cooling system in the fiber spectrometer, make difficult or even impossible to realize *in situ* PL spectroscopy with the current components even if there are many nanowires luminescing in the flow. For future PL experiments I would like to suggest to build a novel luminescence detection scheme using a normal avalanche detector or photo multiplier tube, in which the luminescence would be collected and converted to an electrical signal. This would give a broad information about the

PL efficiency of the nanowire, which is directly related to the quality of material. Of course, it would have to be tried before we find out its feasibility.

References

1. Streetman, B., G. *Solid State Electronic Devices*. (Prenticr-Hall International,Inc., 1990)
2. Saleh, B. E. A., *Teich M. C. Fundamentals of Photonics* (Wiley, 1987)
3. Astromskas, G. Electrical Characterization of Integrated InAs nano-structures. PhD thesis, Lund University (2010)
4. Dasgupta, N. P. et al. 25th anniversary Article:Semiconductor Nanowires – Synthesis, Characterization, and Applications *Adv. Mater*. **26**, 2137-2184 (2014)
5. Jacobsson, D., Crystal Structures in GaAs Nanowires. PhD Thesis, Lund University (2015)
6. Anttu, N., Nanophotonics in absorbing III-V nanowire arrays. PhD thesis, Lund University (2013)
7. Ganjipour B. Quantum Transport in Heterostructure Nanowires Devices. PhD thesis, Lund University (2014)
8. Anttu, N. et al. Absorption of light in InP nanowire arrays. *Nano Res*. **7**, 816-823 (2014)
9. Heurlin, M. et al. Continuous gas-phase synthesis of nanowires with tunable prperties. *Nature* **492**, 90–94 (2012)
10. Yang, F. et al. Zn-doping of GaAs nanowires grown by Aerotaxy. *J. Cryst. Growth* **414**, 181-186 (2014)
11. Cao, L. et al. Engineering light absorption in semiconductor nanowire devices. *Nature* **8**, 643-647 (2009)
12. Yu, Y., Cao, L., Coupled leaky mode theory for light absorption in 2D, 1D, and 0D semiconductor nanostructures. *Optics Express* **20**, 13847-13856 (2012)
13. Brönstrup, G. et al. Optical Properties of Individual Silicon Nanowires for Photonic Devices. *ACS Nano* **4**, 7113-7122 (2010)
14. Sze, S. M. *Semiconductor Devices: Physics and technology* (John Wiley & Sons,Inc,)
15. Ruda, H.E, Shik, A. Polarization-sensitive optical phenomana in semiconducting and metallic nanowires. *Phys. Rev. B: Condens. Matter* **72**, 115308-1 - 115308-11 (2005)
16. Landau, L.D., Lifshitz E.M., *Electrodynamics of Continuous Media.*(Pergamon Press, 1963)
17. Shik, A. et al Electromechanical and electro-optical properties of nanowires. *J. Appl. Phys* **98**, 094306-1 - 094306-6 (2005)
18. Kim, S. H. et al. Understanding ion-mobility and transport properties of aerosole nanowires. J. Aerosol Sci 38, 823-842 (2007)
19. Fushs, N. A. The mechanics of aerosols. (Oxford:Pergamon Press Ltd.1964)
20. Cao, L. et al. Resosant Germanium Nanoantenna Photodetectors. Nano Lett. 10 1229-1233 (2010)
21. Cao, L. et al. Tuning the Color of Silicon Nanostructures. Nano Lett. 10, 2649-2654 (2010)
22. Hosseinnia, A., Absorption of light through isolated and coupled resonances in horizontal InP nanowire arrays. Master Thesis, Lund University (2014)
23. Grzela, G., et al. Nanowire Antenna Absorption probed with Time Reversed- Fourier Microscopy. *Nano Lett.* **14**, 3227-3234 (2014)
24. Cao, L., et al. Tuning Light the Color of Silicon Nanostructures. *Nano Lett.***10**, 2649-2654 (2010)
25. Choi, D. S., et al Scattering Intensity and Directionality Probed Along Individual Zinc Oxide Nanorods with Precisely Controlled Light Polaarization and Nanorod Orientation. *Photonics* **2**, 684-701 (2015)

26. Gilliland, G. D. Photoluminescence spectroscopy of crystalline semiconductors. *Mater. Sci. Eng., R* **18**, 99-399 (1997)a
27. [http://ecee.colorado.edu/~bart/book/eband5.htm]
28. Metaferia, W. et al. GaAsP Nanowires Grown by Aerotaxy. *Nano Lett.* **16**, 5701–5707 (2016)
29. Magnusson, M., H., et al.Gold Nanoparticles: Production, Reshaping, and Thermal Charging. *J. Nanopart. Res*. **1**, 243-251 (1999)
30. Huang, X., et al. Gold nanoparticles: Optical properties and implementation in cancer diagnosis and photothermal therapy. *JAR **1**,13-28 (2010)*